REPUBLIQUE ALGERIENNE DEMOCRATIQUE ET POPULAIRE
MINISTERE DE L'ENSEIGNEMENT SUPERIEURE ET DE LA RECHERCHE SCIENTIFIQUE

UNIVERSITE ABOU-BEKR BELKAID - TLEMCEN

MEMOIRE

Présenté à :

FACULTE DES SCIENCES – DEPARTEMENT DE PHYSIQUE

MASTER EN PHYSIQUE

Spécialité : Physique des Plasmas

Par :

Melle BERHAB RAHMA

Sur le thème :

Etude de l'interaction Laser attoseconde Matière: Equation de Schrödinger

---

Soutenu publiquement le 10 Juin 2024 à Tlemcen devant le jury composé de :

DIAF NADIA	Maître Assistante	Université de Tlemcen	Présidente
SENOUDI ASSIA RACHIDA	Maître de Conférences (A)	Université de Tlemcen	Encadrante
INAL MOKHTAR KAMEL	Professeur	Université de Tlemcen	Examinateur

BERHAB/2024

Année Universitaire : 2023 ~ 2024

Acknowledgements

This master dissertation was realized at the laboratory of theoretical Physics, Physics department, the Faculty of Science of Abu Bakr Belkaid University.

I would like to express my deepest gratitude to my supervisor, Dr. Senoudi Assia Rachida, for her support, invaluable guidance, and continuous encouragement throughout the course of this work.

I am also grateful to the members of the jury, Mme DIAF Nadia, the president of Jury and Professor INAL Mokhtar, the examiner, for their time, constructive comments, and suggestions, which will greatly contributed to the improvement of this work.

I would like to thank the Physics department at the faculty of sciences of Abu Bakr Belkaid University of Tlemcen and the plasma team at the theoretical physics laboratory.

Dedications

First and foremost, I am deeply thankful to Allah for providing me with the strength, wisdom, and perseverance to complete this work.

This work is dedicated to my parents for their unconditional love and support, to my siblings, and to my whole family for their constant encouragement and understanding.

A special thanks to my friends and colleagues for their support and guidance.

Lastly, I would like to dedicate this research to the people of Palestine, in solidarity with their suffering, with hopes for their future peace and FREEDOM.

CONTENTS

General Introduction

The ability to observe and manipulate phenomena on ultrashort timescales has been a crucial matter for scientists. From the groundbreaking microsecond imagery captured by Harold "Doc" Edgerton in the early 20th century, which famously froze a bullet piercing an apple mid-flight, to the development of picosecond and then femtosecond lasers in the 1970s–1980s thanks to the pioneering work of Erich Ippen and Herman Haus at MIT (Massachusetts Institute of Technology), and Chuck Shank at Bell Laboratories, each leap in temporal resolution has revealed new aspects of the physical world [1].

The cutting edge of this exploration now lies in attoscience, a field dedicated to studying events that unfold in attoseconds (10^{-18} s),which is the timescale of the most elementary electronic dynamics in atoms, molecules, but also solid state. According to the Bohr-model of hydrogen atom, an electron in the ground state moves in a circular classical orbit around the nucleus in approximately 150 as. Decades of technological advancements and extensive researches have now made it possible to generate pulses lasting less than 100 attoseconds. Last year, Anne L'Huillier, Pierre Agostini and Ferenc Krausz earned the Nobel Prize in Physics for their contributions to the study of electrons. Their approach involves using attosecond-long flashes of light to illuminate molecules, offering a unique perspective on the behavior and characteristics of electrons in molecules, and for understanding fundamental quantum mechanics and chemical reactions [2, 3].

Ultrashort laser pulses, such as femtosecond and attosecond pulses, interact with materials in a unique way due to the extremely brief duration of the energy deposition. When such a pulse illuminates a materiel, the energy from the laser is primarily absorbed by the free electrons, making them the main carriers of the thermal energy. The interaction time of the pulse is comparable to the electron relaxation time, leading to a scenario where the traditional heat conduction models, such as the Fourier equation, fail to accurately describe the thermal energy transfer. The Fourier equation assumes a continuous and gradual propagation of heat, which is appropriate for longer timescales. However, for ultrafast thermal pulses, the situation is different. The hyperbolic nature of thermal energy transfer becomes significant, meaning that the speed of heat propagation is finite and comparable to the speed of the energy carriers, i.e., the electrons. This leads to non-Fourier heat conduction behavior [4].

Objective and Work plan:

Our main objective is to investigate the interaction between matter and attosecond laser pulses to gain more insights into the behavior of electrons under the influence of these ultrashort pulses, we will follow a structured plan of work:

In the first chapter, we have explored the different time scales from milliseconds to attoseconds, as well as the dynamics that occur during these time periods. We have provided in detailed explanation, the nonlinear process of generating attosecond pulses (HHG), using a description based on a semi-classical model.

In the second chapter, we have studied the interaction of an attosecond laser with matter, which leads to the propagation of thermal waves in the material that no longer follows Fourier's law. Specifically:

- We introduced the heat transfer model under the influence of attosecond pulses, which is described by the quantum heat transport equation (QHT) and the modified Schrödinger equation (MSE) to analyze the behavior of electrons under attosecond laser.
- We have conducted a theoretical study, including the mathematical derivation of the modified Schrödinger equation (MSE).
- The MSE was solved by separating variables leading to 2 equations: One is temporal differential equation of order 2 and the second is the classical and independent time Schrodinger equation.
- We performed analytical solution of the differential temporal equation of MSE.

In the third chapter:

- We presented the principles of the numerical finite difference method.
- We solved the radial equation of the modified Schrödinger equation describing a hydrogen atom, where the electron is under Coulomb potential.
- We have transformed the problem on the Eigen values form matrix.
- We presented the different scripts which we have written for solving the problem using Python language.
- Wave functions and densities of probabilities are graphically represented for different states corresponding to different angular momentum quantum numbers *l.*
- The radial solution obtained numerically by the finite difference scheme is associated to the analytical solution of temporal part for performing 2D and 3D representation, consistently demonstrate the significant impact of attosecond pulses.

In this work, Python codes have been performed: Total electrical potential for Tunnel effect and Resolution of MSE by finite difference method.

Chapter I: HIGH HARMONICS GENERATION
For Attoseconds (XUV) Laser

Chapter I

I Introduction

The evolution of laser technology from its inception in the late 1950s to its current state represents a captivating journey through time, spanning a vast range of temporal scales – from milliseconds to attoseconds[1]. The first pulsed lasers appeared in the 1960s with durations of several hundreds of microseconds. Over time, advancements led to the development of femtosecond[2] lasers, with pulse durations in the order of femtoseconds by the year 2000. Subsequently, in 2001, a significant breakthrough occurred as researchers successfully generated attosecond pulses. Isolated attosecond pulses were first observed in 2001 by Ferenc Krausz and his team at the Technical University of Vienna using light pulses lasting approximately 650 attoseconds [5]. In 2012, the world record for the shortest light pulse generated by human technology was set at 43 attoseconds. Since then, attosecond technology has advanced quickly contributing to various fields including materials science, biophysics and chemistry. In this chapter, we will present different physical dynamics that can occur within different time scales. Subsequently, we delve into the high harmonics generation (HHG), source of attosecond pulses laser. We used the semi-classical model for describing the processes of the HHG. Lastly, we'll discuss some practical uses for these attosecond pulses in various fields.

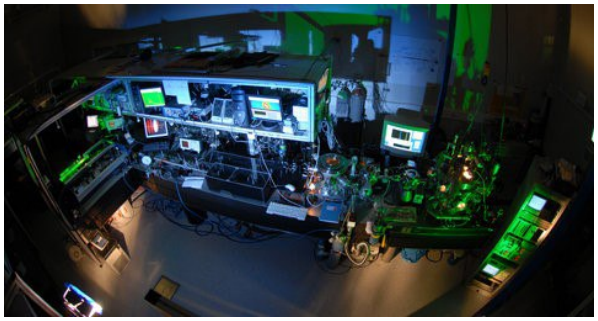

Figure I.1: Ferenc Krausz and his team at the Vienna University of Technology managed to produce attosecond light flashes for the first time in 2001. (Photo by Thorsten Naeser) [5].

[1] $Attoseconds(as) = 10^{-18} seconds$
[2] $Femtoseconds(fs) = 10^{-15} seconds$

II Time Scales

The concept of multiples and submultiples in distance and time of a given unit is fundamental for adapting measurements to specific physical quantities. Temporal intervals ranging from fractions of seconds to years align with human capabilities and their perception. Also finer gradations such as milliseconds, microseconds, nanoseconds[3] , picoseconds[4] ,femtoseconds, attoseconds, and even zeptoseconds[5] have been defined to address specific dynamics within various contexts. Each unit finds relevance in understanding and quantifying distinct phenomena at different temporal scales [6].

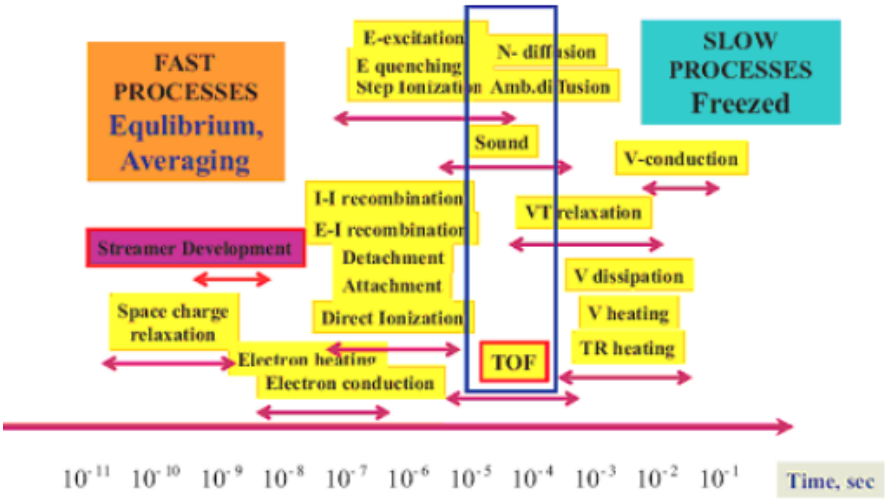

Figure I.2: Time scales for different processes in the plasma [7]

II.1 Millisecond

We cite some fields where the milliseconds are a time duration scale:

- Fluid dynamics : Some processes involving turbulence phenomena cause the fluid to fragment into drops or bubbles within a few milliseconds [8].
- Cellular processes: Neural action potentials generally have duration of about 2 milliseconds.
- Photosynthetic Protein Dynamics: Research has revealed that dynamics within photosynthetic proteins occur at very rapid timescales [9].
- Mechanical systems as example a camera shutter which capture images, opens and closes within a fraction of a millisecond.

[3] $Nanosecond(ns) = 10^{-9} seconds$
[4] $Picoseconds(ps) = 10^{-12} seconds$
[5] $Zeptoseconds(zs) = 10^{-21} seconds$

II.2 Microsecond:

- Air vibrations: Acute sounds associated with explosions or high-frequency events, have durations of the order of microseconds[10].
- Access time to electronic memories: The time delay between a request to an electronic system and the returned data is of 10 microseconds [11].

II.3 Nanosecond

- Electronic Junctions: the switching time of transistors and other electronic components often occurs within the nanosecond time, as example, 35 ns for the 2N3904 transistor [12].
- - Cycle Time of Computers: It represents the duration time for one instruction to be executed. It is measured in nanoseconds.
- Molecular biology: Nanoseconds are a timescale for understanding the dynamics and rearrangements of protein structures [13].

II.4 Picoseconds

- In semiconductor devices: the movement of electrons and holes within the material is extremely fast, and this motion is governed by picosecond and femtosecond time scales [14].
- Some chemical reactions can also take place on these short time scales.

II.5 Femtoseconds

- This timescale is typical for nuclei dynamics fundamental to chemistry. In a molecule, atoms can move and turn in few fs. The fundamental mode of vibration of molecular di-hydrogen has a period of 8 fs.

Some researchers at the FERMI investigated a photochemical reaction using high-resolution photoelectron spectroscopy. They focused on acetylacetone (a stable molecule with several applications). Their method allowed them to observe rapid changes in the molecule's electronic and geometric structure on a femtosecond timescale. This approach offers insights into fundamental photochemical processes like photosynthesis and photovoltaic energy production [15]. High-energy X-ray pulses with femtosecond duration could make it possible to obtain detailed images, and ultimately movies, of the dynamics of complex protein molecules.

II.6 Attosecond

Attoseconds is the time scale of the most elementary electronic dynamics in atoms, molecules, but also solid state. According to the Bohr-model of hydrogen atom, an electron in the ground state moves in a circular classical orbit around the nucleus in approximately 150 as. At the attosecond timescale, several key electronic dynamics occur, including:

- Electron Tunnelling: Electrons can tunnel through potential barriers, a phenomenon fundamental to processes like quantum tunnelling microscopy and field emission.

- Photoionization: When atoms or molecules absorb photons, electrons can be ejected from the system in a process known as photoionization. We can observe this phenomenon at attosecond timescales

- Attosecond Charge Migration:In molecules, charge migration processes can occur on the attosecond timescale, where electrons redistribute due to the influence of the laser field or other environmental factors [16].

- Ultrafast Energy Transfer:In complex systems such as biomolecules or solid-state materials, energy transfer processes can occur on attosecond timescales.

- Coherent Electron Motion:Attosecond pulses of light can induce coherent motion of electrons within atoms or molecules. This includes processes such as the generation of high-harmonic radiation or the coherent control of electronic wave pack [17].

III Generation of attosecond pulses

In 1988, physicists at CEA-Saclay discovered that by exciting atoms of rare gases with short and intense laser pulses, a large number of frequencies, all multiples of the initial laser frequency, known as harmonic frequencies, were emitted. Using an infrared laser, (TiSaphire) they were able to generate radiation covering a broad spectrum of frequencies, from visible light to X-rays.

At that time, the synchronization of these harmonic frequencies remained an open question as no technique existed to measure it. In 1993, Paul Corkum proposed a model where the production of these harmonics was associated with the emission of ultra-short pulses. This process can be very well understood in the framework of the semi classical three step model.

III.1 Three Step Model

The generation of attosecond pulses involves using intense lasers (Femtosecond pulses, see Figure I.2) to ionize a medium, leading to the emission of high-energy photons in the extreme ultraviolet (XUV) or X-ray range through a process called high harmonic generation (HHG) (Figure I.3). These XUV pulses are sub-femtosecond in duration. The energy required for this process is quantified by the ponderomotive energy of the laser. Although HHG produces sub-femtosecond pulses, specific techniques are needed to isolate individual attosecond pulses, often used for high-resolution temporal experiments.

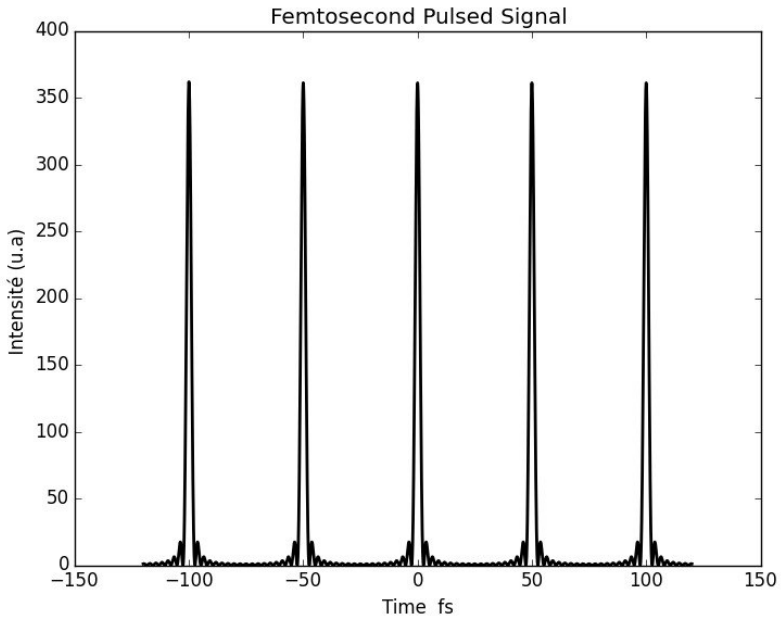

Figure I.3: Femtosecond pulses computed by Python code [Annex 1] Source laser generating the HHG

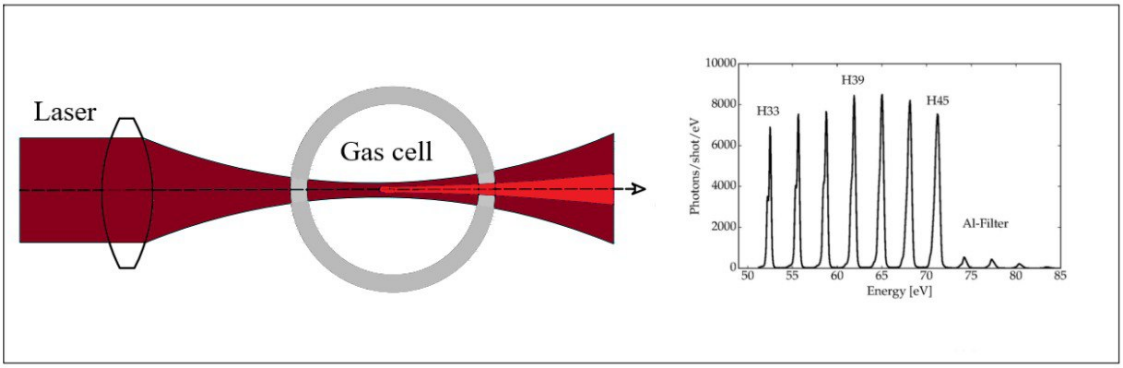

Figure I.4: Schematic of a High Harmonic Generation (HHG) setup along with a typical harmonic spectrum. The abscises is labelled in terms of multiples of the energy of the initial photon used for driving, indicating different harmonic orders.(Spectrum of a neon HHG source driven by a Ti-sapphire laser [18]

If we irradiate an atom with an intense oscillating laser field weakly bound electrons may tunnel into the continuum. The guided electronic wave packet may recombine with the ion,emitting kinetic energy as photons. In summary, the three steps involve:

- Tunnelling
- Excursion in the continuum,

- and potential recombination with photon emission.

a.Tunnel ionization

When a femtosecond laser pulse is directed towards a gas target, its peak intensity typically falls within the range of 10^{13} and 10^{15} W/cm^2. Under such conditions, the Coulomb potential affecting the outer-shell electrons undergoes significant alteration due to the intense laser electric field. This alteration results in the formation of a potential barrier, enabling electron tunneling to occur.

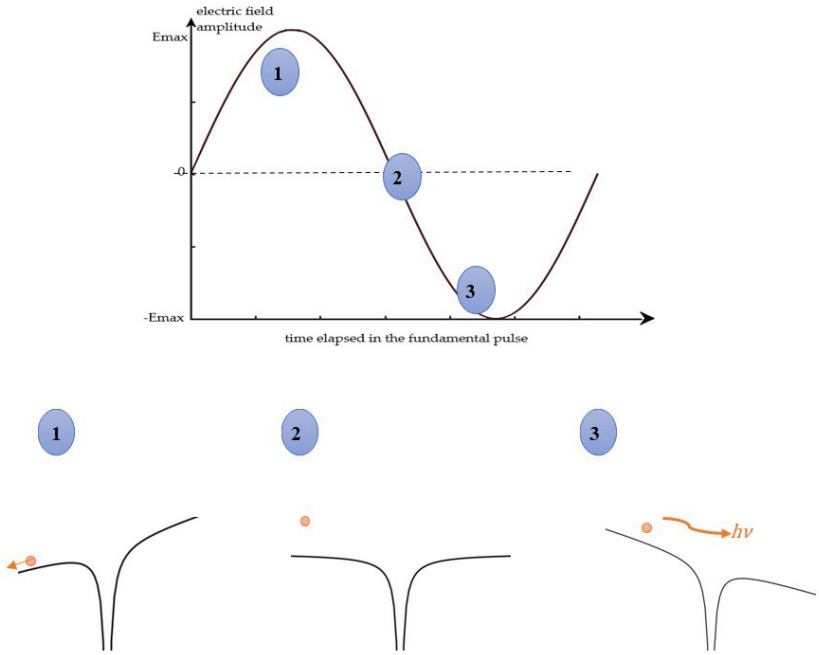

Figure I.5: Three step model of high harmonic generation (HHG). Step one represents tunnel ionization, two represents propagation and three is the recombination. E_{max}= 0.1 (u.a)

- In this step, we consider the potential of the ionic core as a coulomb potential in the form of:

$$V = \frac{Z_{eff}}{|x|} \tag{I.1}$$

- The electric field of the laser:$E(t) = E_0 \cos(\omega t)$ is supposed to be homogeneous on the relevant size scales around the atom. The associated potential is $E_0.x$

- The total electric potential (we put $Z_{eff} = 1$) seen by the electron is :

$$V(x) = -\frac{1}{x} + E_0 \cdot x \tag{I.2}$$

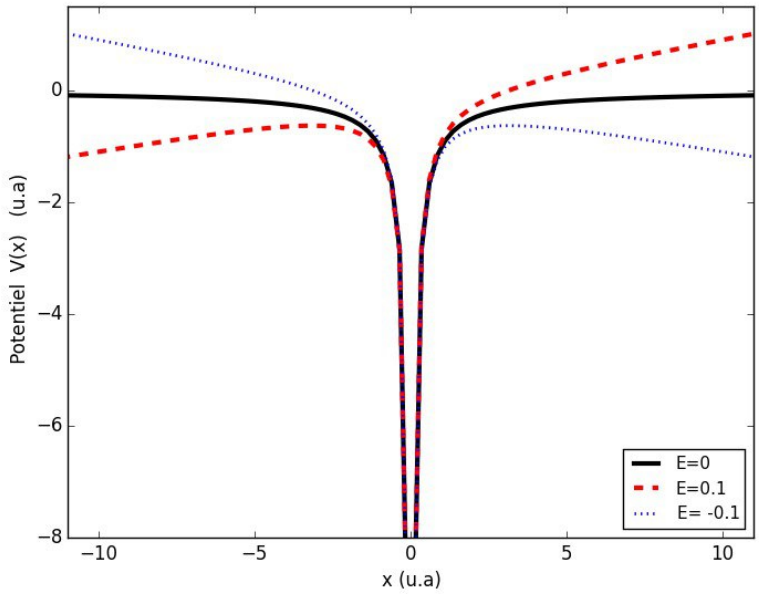

Figure I.6: Total electric potential seen by electron, for $E_0 = 0$, $E_0 > 0$ and $E_0 < 0$ from Python Code we performed [Annex 2]

When the electric field is null, the electron remains bound to the ionic c ore. However, as the electric field o f t he l aser i ncreases, i t c reates a b arrier w hose h eight decreases with the increasing the laser electric field, facilitating electron e scape. The value of the maximum of the barrier is noted V_{xm}, thus if $V_{\text{xm}} <$ Ionization Potential I_p, the electron can directly escape (tunnel) the potential and the atom gets ionized.

If $I_p < V_{\text{xm}} < 0$, classically, an electron would be confined w ithin t he p otential of the ionic core and unable to escape. However, in the realm of quantum mechanics, there exists the possibility of tunnelling, whereby the electron can surpass the potential barrier and ionize. The rate of this tunnelling depends on the width of the barrier, and its height [19].

Let's take the case where the barrier is lowered on the x>0 and by deriving eq. (I.1), we get:

$$\frac{dV}{dt} = \frac{1}{x^2} + E_0 \tag{I.3}$$

$$x_m = \frac{1}{\sqrt{-E_0}} \tag{I.4}$$

When $x_m = l_p$, we have what we call Barrier suppression ionization, this directly leads tothe field strength and corresponding intensity of

$$E_{BS} = \frac{I_p^2}{4}, I_{BS} = \frac{I_p^4}{16}, I_{BS}\left[\frac{\text{W}}{\text{cm}^2}\right] = 4 \times 10^9 \cdot I_p^4 \cdot [\text{eV}] \tag{I.5}$$

Once these intensities are reached, the rate of tunnel ionization becomes notable. The table below represents ionization potential and barrier suppression intensities of noble gases [19]. The table indicates lighter elements with higher ionization potential can stand more laser Intensity.

Gas	I_p (eV)	$I_{BS} \times 10^{14}$ W/cm^2	$E_{BS} \times 10^{10}$ V/m
He	24.58	14.6	10.49
Ne	21.55	8.62	8.06
Ar	15.75	2.46	4.31
Kr	14.00	1.53	3.40
Xe	12.13	0.87	2.55

Table I.1: Gas ionization potentials and related parameters

The Keldysh parameter is introduced as an adiabaticity parameter called "γ", giving an additional criterion for the existence of a tunnel regime. This parameter is defined as the ratio of the time the electron would need to cross the barrier and the laser period:

$$\gamma = \frac{\tau}{T_0} = \sqrt{\frac{I_p}{2U_p}} \tag{I.6}$$

where U_p is the ponderomotive potential,which represents the average kinetic energy of a free electron oscillating in the field. If the laser field exhibits high amplitude and low frequency, the potential barrier remains relatively low for an extended period, and $\gamma \ll 1$ as long as the laser field's intensity remains below E_{BS}. Conversely, when the laser field is weak and has a high frequency,γ becomes significantly larger than 1. In such conditions, tunnel ionization is not efficient [20].

b. Propagation

The ejected electron is accelerated in the continuum, the propagation of this electron can be described classically since we can ignore the coulomb force excreted by the ion, thus the electron's movement can be studied using the classical model of a free electron accelerated in the presence of the electric field of the laser pulse.

We consider the initial conditions: $v(t_0) = 0$ and $x(t_0) = 0$

$$m\frac{dv}{dt} = -eE_0 \cos(\omega t) \tag{I.7}$$

$$v(t) = -\frac{eE_0}{m\omega}\left(\sin\omega t - \sin\omega t_0\right) \tag{I.8}$$

$$x(t) = \frac{eE_0}{m\omega^2}(\cos(\omega t) - \cos(\omega t_0)) + (t - t_0)\frac{eE_0}{m\omega}\sin(\omega t_0) \tag{I.9}$$

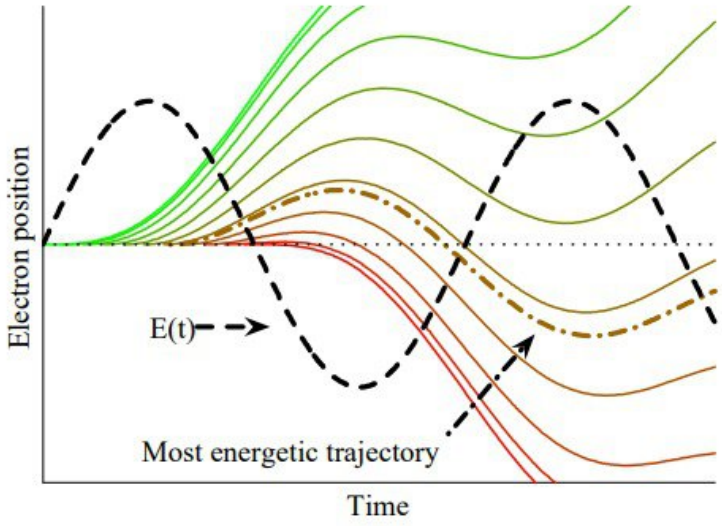

Figure I.7: The electron's position over time varies for different "Ionization times". The term "most energetic trajectory" pertains to the solution in which the electron approaches the nucleus with the highest kinetic energy [21]

c. Recombination

A comprehensive understanding of the recombination stage necessitates a quantum mechanical analysis of the re-scattering[6] and the accompanying radiation emission, through the Schrodinger equation of a single active electron in dipole approximation,

$$i\frac{d}{dt}|\psi\rangle = H|\psi\rangle - \vec{r}.E(t)|\psi\rangle \tag{I.10}$$

$$H = -\frac{1}{2}\nabla^2 + V(\mathbf{r}) \tag{I.11}$$

H is the atomic Hamiltonian, $V(r)$ the effective atomic potential confining the electron to the atom. The energy liberated during recombination can plausibly be equivalent to the sum of the kinetic gained by the electron and the ionization potential, as the electron transitions from the continuum to a state with energy of $-I_p$. In particular, the maximum energy released during the collision can be anticipated to be,

$$\omega_{max} = I_p + 3.17U_p \tag{I.12}$$

This process is repeated periodically every half cycle of the external laser field, and this periodicity corresponds to the emission of the odd harmonics of the fundamental driving wavelength in the spectral domain. Correspondingly, in the temporal domain, harmonics are emitted as a train of attoseconds pulses eparated by half the period of the driving field [21].

[6]The re-scattering problem refers to the phenomenon in quantum mechanics where an electron, after being ionized from an atom or molecule, is subsequently scattered back towards the ion from which it originated.

IV Quantum Description of High-order Harmonic Generation

The semi classical model offers a convenient framework for understanding experimental observations, but its reliance on classical physics is not fully justified. Instead of envisioning an electron as a point particle following a trajectory and emitting light upon bouncing off its parent ion, the more accurate description involves considering the electron as a wave function confined within an atom or molecule.
When subjected to a strong laser field, this wave function undergoes significant deformation.Portions of the wave function are pulled away from the binding potential, traversing classically forbidden barriers. Eventually, these separated parts of the wave function interfere with each other, leading to complex interference patterns. This description better captures the quantum mechanical nature of electron behavior in the presence of strong external fields, contrasting with the simplistic classical trajectory model. In this case we will have the following equation:

$$i\frac{\partial}{\partial t}\psi(\mathbf{r},t) = \left(-\frac{1}{2}\nabla^2 + V_0(r) + \mathbf{r}\cdot E(t)\right)\psi(\mathbf{r},t) \tag{I.13}$$

where $E(t)$ is the external electric field (the laser source) and $V_0(r)$ represents the interaction of the electron with the nucleus shieldedby the remaining bound electrons. Lowenstein et al. proposed an approximate solution build upon the strong-field approximation (SFA) of the Time-Dependent Schrödinger Equation (TDSE), as introduced by Keldysh. This approach simplifies the problem by making several key assumptions [20]:

- Only the ground state of the atom or molecule is taken into account. Any other bound states are disregarded. This simplification reduces the complexity of the system under consideration.
- The effect of the core-potential $V_0(r)$ on the electron in the continuum is assumed to be negligible. In other words, the interaction between the electron and the laser field $\mathbf{r}.E(t)$ is considered dominant compared to the influence of the core potential.

V Attosecond laser applications

The attosecond pulses have found extensive applications across diverse scientific disciplines due to their ability to probe ultrafast dynamics at the atomic and molecule level as we have seen before. We can encounter attosecond laser in many applications such as:
- Attosecond movies of electrons, created through pump-probe spectroscopy, capture electron motion inside atoms. A "pump" pulse initiates movement, while a "probe" pulse illuminates' electrons at various intervals, acting as frames in a conventional movie. Sophisticated detectors gather data on electron behavior, which is then stitched together to form movies. These insights aid in understanding fundamental electronic behavior on attosecond scales, offering potential for controlling electric currents at the molecular level [22].

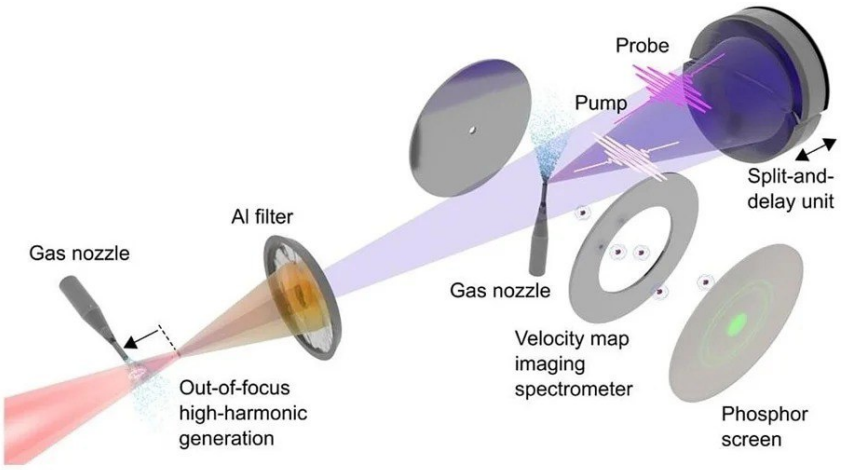

Figure I.8: Experimental setup for attosecond-pump attosecond-probe spectroscopy.Image Credit: Max Born Institute [23]

Gaining a fundamental understanding of a process typically leads to control that process, and such control paves the way for the development of innovative technologies.
- Ultrafast Switches: The capability to modify electron behavior at attosecond timescales could lay the foundation for next-generation ultrafast switches, enabling electronics to operate at speeds far beyond current limits. This has the potential to revolutionize information processing and communication technologies, leading to faster and more efficient devices.
- Chemical Reactions Control: By understanding and controlling electron behavior, researchers can manipulate chemical reactions; this could lead to the creation of novel molecules with unique properties, advancing fields such as materials science, drug discovery, and catalysis.
- One of the very promising applications is attosecond-scale magnetism, where spin dynamics are induced by ultrafast lasers in magnetized materials. This field emerged initially in the femtosecond regime (ultrafast data storage) and is now being pursued towards attosecond regimes. These applications, along with the attosecond precision now achievable, have led to very fundamental questions, such as understanding the non-trivial connections between delays, time, and phase shifts.
- In EUV (Extreme Ultraviolet) lithography, attosecond pulses enable the production of smaller, more advanced electronic chips, enhancing device performance [24].

REFERENCES OF Chapter Ⅰ:

[1] David L. Chandler," Explained: Femtoseconds and attoseconds", MIT News Office (2012).
[2] The Nobel Prize in Physics 2023. NobelPrize.org. Nobel Prize Outreach AB (2024). https://www.nobelprize.org/prizes/physics/2023/summary/
[3] Ferenc Krausz, "The birth of attosecond physics and its coming of age", Phys. Scr. 91 (2016) 063011.
[4] Kozłowski, Miroslaw and Marciak-Kozlowska, J. and Pelc, M. (2008). Attoscience, p.18 https://doi.org/10.48550/arXiv.0806.0165
[5]"Nature Milestones" Photons, Presse- und Öffentlichkeitsarbeit/Max-Planck-Institut für Quantenoptik, (2010).https://www.mpq.mpg.de/4881414/10_05_17
[6] Rethfeld, B., Sokolowski-Tinten *et al*. "Timescales in the response of materials to femtosecond laser excitation", *Appl. Phys. A* 79, 767–769 (2004).
[7]Son, Eduard &Tereshonok, Dmitry. (2010). Thermal and plasma flow control. Physica Scripta. 2010. 014039. 10.1088/0031-8949/2010/T142/014039.
[8] Jay Boris and Keith Obenschain,"Mixing Delays in Non-Equilibrium High-Speed Turbulence", (2022),Naval Research Laboratory,https://apps.dtic.mil/sti/trecms/pdf/AD1161951.pdf
[9] Kondo, T., Gordon, J. B., Pinnola, A., Dall'Osto, L., Bassi, R., & Schlau-Cohen, G. S. (2019). Microsecond and millisecond dynamics in the photosynthetic protein LHCSR1 observed by single-molecule correlation spectroscopy. *Proceedings of the National Academy of Sciences of the United States of America*, *116*(23), 11247–11252. doi:10.1073/pnas.1821207116
[10] Rolling vs global shutter. (2024):https://www.photometrics.com/learn/white-papers/rolling-vs-global-shutter
[11] Time access: http://www.pcmag.com/encyclopedia/term/access-time
[12] Transistor Switching Times. (2019)http://www.eeeguide.com/transistor-switching-times/
[13] Okan, O. B., Atilgan, A. R., &Atilgan, C. (2009). Nanosecond motions in proteins impose bounds on the timescale distributions of local dynamics. *Biophysical Journal*, *97*(7), 2080–2088. doi:10.1016/j.bpj.2009.07.036
[14] Liu, RY., Ogawa, Y., Chen, P. et al. "Femtosecond to picosecond transient effects in WSe 2 observed by pump-probe angle-resolved photoemission spectroscopy". Sci. Rep. 7, 15981 (2017).
[15] Molecular dynamics on the femtosecond timescale. (2018).
https://lightsources.org/2018/01/25/molecular-dynamics-on-the-femtosecond-timescale/
[16] He, L., Sun, S., Lan, P. et al. "Filming movies of attosecond charge migration in single molecules with high harmonic spectroscopy". Nat. Commun 13, 4595 (2022). https://doi.org/10.1038/s41467-022-32313-0)
[17] Aderonke S. Folorunso, Adam Bruner and al." Molecular Modes of Attosecond Charge Migration", Phys. Rev. LETTERS 126, 133002 (2021).
[18] Spectrum of a neon HHG source driven by a Ti-sapphire laser:
https://en.wikipedia.org/wiki/File:Hhg_spec_neon.pdf
[19]DivekiZsolt," Generation and Application of Attosecond Pulses",these doctorate Laser and matter. Université Paris Sud (2011).
[20] Stefan Haessler, "Generation of Attosecond Pulses in Atoms and Molecules",these doctorate Atomic Physics. Université Paris Sud (2009).
[21]High Harmonic Generation:
https://ufox.cfel.de/sites/sites_cfelgroups/site_cfelufox/content/e16281/e86791/e86828/e86829/e86835/UFSIMPRS_HHGsection.pdf
[22] Niranjan Shivaram, "Making movies at the attosecond scale helps researchers better understand electrons – and could one day lead to super-fast electronics", (2023), https://theconversation.com/
[23]MBI / Mikhail Volkovhttps://www.eurekalert.org/multimedia/1016277
[24] Knut and Alice Wallenberg, the world's shortest light pulses and what they can do: https://kaw.wallenberg.org/en/research/worlds-shortest-light-pulses-and-what-they-can-do

Chapter II:Quantum Heat and Modified Schrodinger Equations

Chapter II

I Introduction

Laser pulses interact with materials through multiple mechanisms, leading to a variety of phenomena ranging from electromechanical effects to photothermal processes. For example, femtosecond laser pulses exhibit unique dynamics when interacting with materials compared to longer pulse durations.

In femtosecond laser excitation, fundamental processes like energy deposition, melting, and ablation occur in distinct temporal phases due to the short duration of the pulses. Initially, the laser pulse rapidly deposits a significant amount of energy into a small volume of the material within femtoseconds, leading to localized heating and excitation of electrons. This energy deposition results in fast melting of the material, but due to the short pulse duration, heat diffusion into the bulk is minimal, confining the melting to a thin layer near the surface. Subsequently, before significant heat transfer to the surrounding material can occur, intense energy absorption leads to rapid vaporization or ablation of the material within femtoseconds to picoseconds. This temporal separation allows for precise control over material processing, facilitating applications such as laser micromachining, surface structuring, and ultrafast spectroscopy techniques for studying material properties [1].

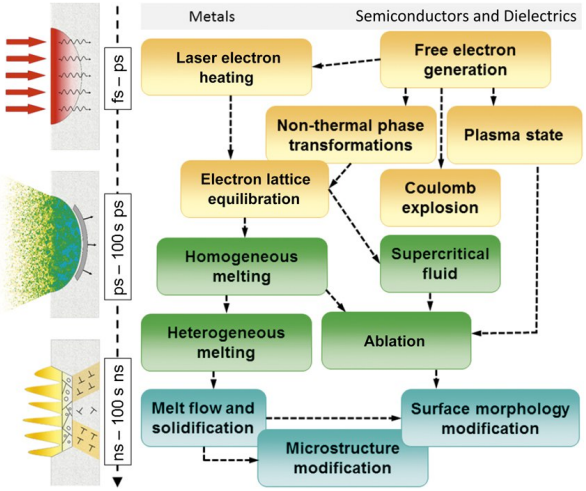

Figure II.1: Ultrafast laser–matter interaction pathways for different materials [2]

The development of femtosecond and attosecond laser technology has reshaped the study of laser-material interactions. However, it also presents obstacles to conventional models relying on the Fourier law of heat conduction.

In addressing these challenges, the Quantum heat equation emerges as a powerful tool for modeling the propagation of thermal waves induced by ultrafast laser pulses. Unlike traditional diffusion models, which assume equilibrium conditions, the hyperbolic nature of this equation captures the transient behavior of heat transport in materials subjected to ultrafast laser irradiation [3].

This chapter explores how attosecond laser pulses interact with matter, enabling the study of electron dynamics using the Modified Schrödinger Equation (MSE). The MSE is a valuable tool for investigating electron behavior in these conditions, by applying the MSE, we aim to gain deeper insights into how electrons behave in atomic systems under attosecond laser influence.

II Quantum Heat Transport Equation (QHT)

The wave model of heat transfer offers a different perspective compared to classical heat diffusion theory by recognizing that heat doesn't instantly spread through solids but rather moves at a finite speed. This understanding changes how we think about heat transfer, mathematically rendering the energy equation hyperbolic in nature. In this model, the speed at which thermal waves move is crucial, acting like the speed of a traveling wave, while thermal diffusivity acts as a damping factor in the propagation of thermal waves. The balance between these two factors is measured using the concept of relaxation time within the wave theory framework.

The classical diffusion theory is considered a special case where the relaxation time is zero, implying immediate response to changes in temperature. Conversely, the wave theory accounts for the relaxation behavior in the history of thermal wave propagation. Both temperature and flux waves exhibit a common characteristic of sharp wave fronts when traversing through a solid medium. This phenomenon leads to the formation of thermal shocks, which is a notable aspect addressed by the wave theory [4].

According to the constitutive relation in the thermal wave model, heat flux $\vec{q}$ obeys the relation [5]:

$$\mathbf{q}(\mathbf{r}, t+\tau) = -k\nabla T(\mathbf{r}, t) \tag{II.1}$$

Where τ is the relaxation time, represents the timescale over which an atom or molecule typically returns to its equilibrium state following an external perturbation, and k represent the thermal conductivity.
The temperature gradient at time t causes a heat flux at a later time $t+\tau$ due to delayed response. To incorporate this into the energy equation, all involved physical quantities must correspond to the same time instant. We apply the Taylor's series expansion to the heat flux in Eq. (II.1):

$$\mathbf{q}(\mathbf{r}, t) + \tau\frac{\partial \mathbf{q}(\mathbf{r}, t)}{\partial t} + \frac{\tau^2}{2}\frac{\partial^2 \mathbf{q}(\mathbf{r}, t)}{\partial t^2} + \ldots = k\nabla T(\mathbf{r}, t) \tag{II.2}$$

The relaxation time is assumed to be small, thus we can neglect the higher order terms of τ, eq. (II.2) becomes:

$$\mathbf{q}(\mathbf{r},t)+\tau\frac{\partial\mathbf{q}(\mathbf{r},t)}{\partial t}=k\nabla T(\mathbf{r},t) \tag{II.3}$$

The energy equation:

$$-\nabla\mathbf{q}+S=\rho C_p\frac{\partial T}{\partial t} \tag{II.4}$$

Where S represents the laser source energy, which serves as the heat source, ρ is the mass density, and C_p is the heat capacity.
We combine eq. (II.3) with eq. (II.4) by eliminating $\vec{q}$ from the two equations and we applythe divergence operator to eq. (II.3):

$$\nabla\cdot\mathbf{q}(\mathbf{r},t)+\tau\nabla\frac{\partial\mathbf{q}(\mathbf{r},t)}{\partial t}=k\nabla^2T(\mathbf{r},t) \tag{II.5}$$

Then, we derive eq. (II.4) with respect to time we get:

$$-\frac{\partial}{\partial t}\nabla\mathbf{q}+\frac{\partial S}{\partial t}=\rho C_p\frac{\partial^2T}{\partial t^2} \tag{II.6}$$

We get from eq. (II.4):

$$\nabla\mathbf{q}=S-\rho C_p\frac{\partial T}{\partial t} \tag{II.7}$$

And from eq. (II.6):

$$\frac{\partial}{\partial t}\nabla\mathbf{q}=\frac{\partial S}{\partial t}-\rho C_p\frac{\partial^2T}{\partial t^2} \tag{II.8}$$

By replacing eqs. (II.7) and (II.8) in eq. (II.5) we obtain:

$$D_T\nabla^2T+\left(\frac{1}{\rho C_p}\right)\left(S+\frac{D_T}{vh^2}\frac{\partial S}{\partial t}\right)=\frac{D_T}{vh^2}\frac{\partial^2T}{\partial t^2}+\frac{\partial T}{\partial t} \tag{II.9}$$

$$D_T\nabla^2T-\frac{D_T}{vh^2}\frac{\partial^2T}{\partial t^2}-\frac{\partial T}{\partial t}=-\left(\frac{1}{\rho C_p}\right)\left(S+\frac{D_T}{vh^2}\frac{\partial S}{\partial t}\right) \tag{II.10}$$

$$D_T\nabla^2T-\frac{D_T}{vh^2}\frac{\partial^2T}{\partial t^2}-\frac{\partial T}{\partial t}=f(t) \tag{II.11}$$

If we consider a medium without a source (we ignore the second term of (II.10) noted $f(t)$), the eq. (II.11) becomes:

$$\frac{1}{vh^2}\frac{\partial^2T}{\partial t^2}+\frac{1}{D_T}\frac{\partial T}{\partial t}=\nabla^2T, D_T=\tau vh^2 \tag{II.12}$$

with D_T representing the thermal diffusion coefficient, and v_h the thermal wave velocity.
We can also write eq. (II.12) in the following form:

$$\frac{\partial^2T}{\partial t^2}+\frac{1}{\tau}\frac{\partial T}{\partial t}=\frac{D_T}{\tau}\nabla^2T \tag{II.13}$$

The eq. (II.13) is called the quantum heat transport equation (QHT) [6].
The QHT derives its quantum nature primarily from the intrinsic presence of Planck's constant in the relaxation time that represents a cornerstone in quantum mechanics.
Quantum heat transport equation describes the quantum limit of heat transport when the pulse duration Δt of source laser is of the order or smaller than the relaxation time τ.

III Modified Schrodinger Equation

The conventional Schrödinger equation has been highly successful in describing the behavior of atoms, molecules, and solids under normal conditions. However, its applicability diminishes when confronted with phenomena occurring at the attosecond scale, where ultrafast dynamics unfold.

To describe the behavior of matter under the irradiation of attosecond laser pulses, a modified Schrödinger equation is proposed. This modified equation would account for the ultrafast dynamics and short time periods involved. It may include additional terms or modifications to the original equation to accurately capture the behavior of particles under such extreme conditions[7] .

The Fourier equation for $\tau = 0$ and the Schrödinger equation are both parabolic equations [8]:

$$\frac{1}{D_T}\frac{\partial T}{\partial t} = \nabla^2 T \tag{II.14}$$

$$i\hbar\frac{\partial \psi}{\partial t} = -\frac{\hbar^2}{2m}\nabla^2\psi \tag{II.15}$$

We apply the following complex transformation : $t \leftrightarrow it, \quad \Psi \leftrightarrow T$

It was proven in [9] that when applying this complex transformation, fundamental equations in physics exhibit invariant behavior.

We can rewrite Fourier equation as:

$$i\hbar\frac{\partial \psi}{\partial t} = -D_T\hbar\nabla^2\psi \tag{II.16}$$

By identification with the Schrödinger equation, we obtain:

$$D_T = -\frac{\hbar}{2m} \tag{II.17}$$

Since $D_T = \tau v_h^2$,we obtain the form of the relaxation time for quantum thermal processes directly from (II.17) :

$$\tau = \frac{\hbar}{2mv_h^2} \tag{II.18}$$

Now let's take the case where the particle with mass m is in potential V, the Schrödinger equation becomes:

$$i\hbar\frac{\partial \psi}{\partial t} = -\frac{\hbar^2}{2m}\nabla^2\psi + V\psi \tag{II.19}$$

And by using the previous substitutions, we get:

$$\frac{\partial T}{\partial t} = \frac{\hbar}{2m}\nabla^2 T - \frac{V}{\hbar}T \tag{II.20}$$

For $\tau \neq 0$, the eq. (II.20) becomes:

$$\tau\frac{\partial^2 T}{\partial t^2} + \frac{\partial T}{\partial t} + \frac{V}{\hbar}T = \frac{\hbar}{2m}\nabla^2 T \tag{II.21}$$

With the same substitutions eq. (II.21) can be rewritten as,

$$i\hbar\frac{\partial \psi}{\partial t} = -\frac{\hbar^2}{2m}\nabla^2\psi + V(\mathbf{r})\psi - \tau\hbar\frac{\partial^2\psi}{\partial t^2} \tag{II.22}$$

The eq. (II.22) represents the modified Schrödinger equation (MSE).
As a conclusion, the quantum heat transport equation (QHT) leads to the modified Schrödinger equation.

To solve the MSE, we often adopt spherical coordinates. This choice stems from the prevalent symmetry in atomic and molecular systems, thus eq (II.22) takes the following form:

$$i\hbar\frac{\partial\psi(\vec{r},t)}{\partial t} = -\frac{\hbar^2}{2m}\nabla^2\psi + V(r)\psi(\vec{r},t) - \tau\hbar\frac{\partial^2\psi(\vec{r},t)}{\partial t^2} \tag{II.23}$$

The wave function $\psi(\vec{r},t)$ can be written as the product of two functions, as the following:

$$\psi(\vec{r},t) = \psi(\vec{r})\varphi(t) \tag{II.24}$$

Substituting (II.24) into eq. (II.23), we obtain:

$$i\hbar\psi(\vec{r})\frac{\partial\varphi(t)}{\partial t} = -\frac{\hbar^2}{2m}\varphi(t)\nabla^2\psi + V(r)\varphi(t)\psi(\vec{r}) - \tau\hbar\psi(\vec{r})\frac{\partial^2\varphi(t)}{\partial t^2} \tag{II.25}$$

$$i\hbar\psi(\vec{r})\frac{\partial\varphi(t)}{\partial t} = \left(-\frac{\hbar^2}{2m}\nabla^2\psi + V(r)\psi(\vec{r})\right)\varphi(t) - \tau\hbar\psi(\vec{r})\frac{\partial^2\varphi(t)}{\partial t^2} \tag{II.26}$$

The time independent Schrodinger equation [Annex 3] can be written as:

$$-\frac{\hbar^2}{2m}\nabla^2\psi + V(r)\psi(\vec{r}) = E\psi(\vec{r}) \tag{II.27}$$

Substituting eq. (II.27) in eq. (II.26), we obtain:

$$i\hbar\psi(\vec{r})\frac{\partial\varphi(t)}{\partial t} = E\psi(\vec{r})\varphi(t) - \tau\hbar\psi(\vec{r})\frac{\partial^2\varphi(t)}{\partial t^2} \tag{II.28}$$

Dividing by $\psi(\vec{r})$:

$$i\hbar\frac{\partial\varphi(t)}{\partial t} + \tau\hbar\frac{\partial^2\varphi(t)}{\partial t^2} = E\varphi(t) \tag{II.29}$$

$$\frac{\partial^2\varphi(t)}{\partial t^2} + \frac{i}{\tau}\frac{\partial\varphi(t)}{\partial t} - \frac{E}{\tau\hbar}\varphi(t) = 0 \tag{II.30}$$

Now to solve the time dependent equation (II.30), we set: $\varphi(t) = e^{yt}$

$$\frac{\partial\varphi(t)}{\partial t} = ye^{yt}; \frac{\partial^2\varphi(t)}{\partial t^2} = y^2e^{yt} \tag{II.31}$$

Substituting the previous first and second derivatives in eq. (II.30):

$$y^2 + \frac{i}{\tau}y - \frac{E}{\tau\hbar} = 0 \rightarrow \tau\hbar y^2 + i\hbar y - E = 0 \tag{II.32}$$

Calculating the discriminan Δ :

$$\Delta = (i\hbar)^2 + 4E\tau\hbar \tag{II.33}$$

$$\Delta = \hbar^2\left(\frac{4\tau E}{\hbar} - 1\right) \tag{II.34}$$

$$y_{1,2} = \frac{-i\hbar \pm \sqrt{\frac{4\tau E}{\hbar} - 1}}{2\tau\hbar} \tag{II.35}$$

$$y_{1,2} = \frac{1}{2\tau}\left(-i \pm \sqrt{\frac{4\tau E}{\hbar} - 1}\right) \tag{II.36}$$

With $E = \hbar\omega$, $\tau = \frac{\hbar}{2mv_0\hbar^2}$ y_1 and y_2 represent the roots of the quadratic equation (II.32).We set:

$$\alpha = \frac{\sqrt{\frac{4\tau E}{\hbar} - 1}}{2\tau} \tag{II.37}$$

The general solution of eq. (II.23) is found:

$$\Psi(\vec{r}, t) = \psi(\vec{r})e^{-i\frac{t}{2\tau}}(Ae^{\alpha t} + Be^{-\alpha t}) \tag{II.38}$$

α can be either be a real number or a complex number:

$$4\tau\frac{E}{\hbar} - 1 > 0 \implies 4\tau\frac{E}{\hbar} > 1 \implies 4\tau\omega > 1 \implies \omega > \frac{1}{4\tau} \tag{II.39}$$

If $\omega > \frac{1}{4\tau}$ then α is a real number;
If $\omega < \frac{1}{4\tau}$ then α is a complex number.
We can arrive to a similar solution obtained in [10], when $4\tau\frac{E}{\hbar} \ll 1$, $\alpha \approx \frac{i}{2\tau}\left(1 - 2\tau\frac{E}{\hbar}\right)$

$$\Psi(\vec{r}, t) = \psi(\vec{r})e^{-i\frac{t}{\tau}}\left(Ae^{-i\left(\frac{Et}{\hbar} - \frac{t}{\tau}\right)} + Be^{i\frac{E}{\hbar}t}\right) \tag{II.40}$$

Interpretation:

The general solution of the MSE is different of the solution of the classical Schrodinger equation.

We observe the presence of common term $e^{-i\frac{t}{\tau}}$ function of the relaxation time τ and characterizing the interaction of electrons with their environment within atoms during the irradiation by attosecond laser. This additive term could be considered as a frictional force suggesting that electrons move within a highly viscous medium, this force remains undetectable for long time pulses $\Delta t >> \tau$, but can be probed using attosecond laser pulses. The modified Schrödinger equation (MSE (eq. II.22)) is reduced to the standard Schrödinger equation, in the limit where the relaxation time approaches zero. This limit implies that for non-zero mass, the velocity $\to \infty$ This behavior is in agreement with the nonrelativistic nature of the Schrödinger equation, where information can propagate with infinite velocity (eq. II.18). In contrast, the MSE allows for the transfer of information with a finite velocity $v = \alpha c$, where $v < c$ .This limitation on the velocity of information propagation is a consequence of the presence of the frictional term and the associated relaxation time [10].

IV Modified Klein-Gordon Equation

In the early 20th century, Schrödinger's equation emerged as a powerful tool for understanding atomic physics, providing a comprehensive framework to describe various phenomena. However, Einstein's theory of special relativity necessitated a unified

framework that could integrate quantum mechanics and relativity. While Schrödinger's equation is adept at describing the behavior of non-relativistic particles, its utility diminishes as particle velocities approach the speed of light.

To address this limitation, the Klein-Gordon equation was introduced, named after physicists Oskar Klein and Walter Gordon [10]. Unlike Schrödinger's equation, the Klein-Gordon equation seamlessly merges quantum mechanics with special relativity. It maintains relativistic invariance, making it essential for accurately describing high-energy phenomena .
This equation is indispensable for analyzing relativistic quantum systems, such as mesons, where conventional approaches fall short.

Through careful analysis, it becomes evident that the hyperbolic quantum heat equation (QHT) can lead to the modified Klein-Gordon equation.
Starting from the eq. (3.9) and considering a one-dimensional case [11]:

$$\tau\frac{\partial^2 T}{\partial t^2}+\frac{\partial T}{\partial t}+\frac{V}{\hbar}T-\frac{\hbar}{2m}\frac{\partial^2 T}{\partial x^2}=0,\quad \tau=\frac{\hbar}{2mv_h^2} \tag{II.41}$$

The general solution of eq. (II.1) can be written as:

$$T(x,t)=e^{-\frac{t}{2\tau}}u(x,t) \tag{II.42}$$

$$\frac{\partial T(x,t)}{\partial t}=e^{-\frac{t}{2\tau}}\left(\frac{\partial u}{\partial t}-\frac{1}{2\tau}u(x,t)\right) \tag{II.43}$$

$$\frac{\partial^2 T(x,t)}{\partial t^2}=e^{-\frac{t}{2\tau}}\left(\frac{\partial^2 u}{\partial t^2}-\frac{1}{\tau}\frac{\partial u}{\partial t}+\frac{1}{4\tau^2}u(x,t)\right) \tag{II.44}$$

$$\frac{\partial^2 T}{\partial x^2}=e^{-\frac{t}{2\tau}}\frac{\partial^2 u}{\partial x^2} \tag{II.45}$$

By replacing eqs. (II.41), (II.42), (II.43) and (II.44) in eq. (II.40), we obtain the following:

$$\frac{1}{v_h^2}\frac{\partial u^2}{\partial t^2}-\frac{\partial u^2}{\partial x^2}+\left(\frac{m^2v_h^2}{4\hbar^2}+\frac{V}{\hbar}\right)u(x,t)=0 \tag{II.46}$$

In the absence of any external potentials, for a relativistic electron, the eq. (II.45) becomes:

$$\frac{1}{v_h^2}\frac{\partial u^2}{\partial t^2}-\frac{\partial u^2}{\partial x^2}-\left(\frac{mv_h}{2\hbar}\right)^2u(x,t)=0 \tag{II.47}$$

Eq. (11.46) represents the modified Gordon-Klein equation which can be rewritten as:

$$\boxed{u}(x,t)-\left(\frac{mv}{2\hbar}\right)^2u(x,t)=0 \tag{II.48}$$

Where $\Box$ is the d'alembert operator defined as:

$$\Box=\frac{1}{v\hbar^2}\frac{\partial^2}{\partial t^2}-\frac{\partial^2}{\partial x^2} \tag{II.49}$$

For ultrashort attoseconds pulses, the QHT equation leads directly to the modified KleinGordon equation. It was proven in [11] that heatons, which are thermal wave packets created by the interaction of attosecond laser pulses with matter, are described by the solution derived from the modified Klein-Gordon equation. The study showed that heatons are non-dispersive when the duration of the laser pulses is on the order of attoseconds.

V Conclusion

In conclusion, the study of the interaction of attosecond pulses with matter has revealed complexities that conventional physical models, such as the Fourier law and Schrödinger equation, are unable to describe. To address these challenges, new equations have been developed, such as the QHT equation, the modified Schrödinger equation, and the modified Klein-Gordon equation. These equations provide a more comprehensive framework for understanding the dynamics of attosecond laser pulses interacting with matter, addressing the importance of relaxation time in governing quantum heat transport within atoms, and the significance of probing electron dynamics on extremely short timescales.

REFERENCES OF Chapter II:

[1] Rethfeld, B., Sokolowski-Tinten, K., von der Linde, D. et al. Timescales in the response of materials to femtosecond laser excitation. Appl. Phys. A 79, 767–769 (2004).

[2] Shugaev, M.v.; Wu, C.; Armbruster, O.; Naghilou, A.; Brouwer, N.; Ivanov, D.S.; Derrien, T.J.Y.; Bulgakova, N.M.; Kautek, W.; Rethfeld, B.; et al. "Fundamentals of Ultrafast Laser–Material Interaction". MRS Bull. 41,960–968, (2016).

[3] M. Kozlowski, J. Marciak-Kozlowska, "Beyond the Fourier Equation: Quantum Hyperbolic Heat Transport", 2 Apr (2003), DOI.org/10.48550/arXiv.cond-mat/0304052

[4] M.N. Ozisik and D.Y. Tzou, (1994)On the wave theory of heat conduction, J. Heat Transf. (ASME), Vol. 116, pp. 526-535.

[5] D. Y. Tzou, "Thermal Resonance Under Frequency Excitations » ASME J. Heat Transfer, 114:310 (1992).

[6] Janina Marciak-Kozlowska and Miroslaw Kozlowski, « From Femto-to Attoscience and Beyond » Lasers and Electro-Optics Research and Technology Series Nova Science Publishers, Incorporated, New York (2009). Chap 1 p7.

[7] Isaac Shnaid, "Modified Schrodinger equation, its analysis and experimental verification", February 8, (2012), DOI.org/10.48550/arXiv.1202.1321

[8] M. Kozlowski, J. Marciak-Kozlowska, Josef Pilsudski "Development of the Schrodinger equation for attosecond laser pulse interaction with Planck gas" Lasers in Engineering vol 20, No 3-4, p 157-166, (2010).

[9] Arbab, A. "Derivation of Dirac, Klein-Gordon, Schrodinger, Diffusion and quantum heat transport equations from a universal quantum wave equation". Europhysics Letters, 92 (2010) 40001. DOi: 10.1209/0295-5075/92/40001

[10] C. Foudas, Advanced Particle Physics, 4th year Physics, Imperial College, Lecture: 5, https://alpha.physics.uoi.gr/foudas_public/APP/Lecture5-Klein-Gordon-Dirac.pdf

[11] Janina Marciak-Kozłowska & Mirosław Kozłowski « Modified schrödinger equation for attosecond laser pulse interaction with matter », Lasers in Engineering, 12:1, 53-58, (2002). DOI: 10.1080/08981500290022770

Chapter 3:

Resolution of MSE and Results

I. Introduction

In the second chapter, we established the modified Schrödinger equation, successfullyseparating time and position variables. This separation enabled us to derive an analytical solution for the time-dependent Schrödinger equation. With the analytical solution in hand, we now turn our attention to solving the radial part of the time-independent Schrödinger equation numerically.

In this chapter 3, our primary focus will be on the numerical solution of the radial Schrödinger equation using the finite difference method. This approach will allow us to discretize the equation and solve it iteratively, providing us with the radial component of the wave function. Additionally, we will incorporate the analytical temporal solution into our numerical program to observe the time evolution and visualize the full wave function as governed by the modified Schrödinger equation

II. Finite Difference Methods

The finite difference method (FDM)dates back to Euler in the late 18th century and was extended to multiple dimensions by Runge in the early 20th century. It became widely used in the 1950s with the development of computers, enabling the solution of complex scientific and technological problems. Over the past five decades, significant theoretical progress has been made in understanding its accuracy, stability, and convergence for partial differential equations [1].

II.1 General principle

FDM allows us to transform continuous problems into discrete ones by discretizing both the spatial and temporal domains. This approach consists on replacing derivatives with finite difference approximations, which leads to a system of algebraic equations that can be easily solved numerically.

This method consists on the following steps:

1. Subdivision of the domain as a grid line on which the equation is defined.
2. Approximate the derivatives at each grid point using values from neighboring grid points.
3. Solve the resulting system of equations.

To illustrate the methodology of FDM, we take an example of a simple function and we approximate its first and second derivatives:

$$f: x \longrightarrow f(x) \tag{III. 1}$$

We subdivide the axis of variables into a number of n points, and in the grid given in Figure III.1, the position *x* becomes x_i and thus corresponds to the *index i*:

$$f(x) = f(x_i) \quad \longrightarrow \quad f_i \tag{III. 2}$$

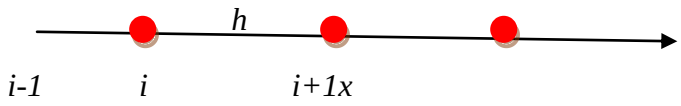

Figure III.1: One-dimensional grid (subdivision), h the step of subdivision

The main idea of finite difference method is to approximate derivatives in the partial differential equations (PDA) by difference quotients, thus we use the formal definition of derivative:

$$\frac{df(x_i)}{dx} = \lim_{h \to 0} \frac{f(x+h) - f(x)}{h} \tag{III. 3}$$

For small values of h, the following quotient is a good approximation of the derivative:

$$\frac{df(x_i)}{dx} \approx \frac{f(x+h) - f(x)}{h} \tag{III. 4}$$

For the second derivative, we use the Taylor expansion, we obtain:

$$\frac{d^2 f(x_i)}{dx^2} \approx \frac{f(x+h) - 2f(x) + f(x-h)}{h^2} \tag{III. 5}$$

Now using the notation in eq. (III.2), we get the following formula:

$$\frac{df(x_i)}{dx} = \frac{f_{i+1} - f_i}{h} \tag{III. 6}$$

$$\frac{d^2 f(x_i)}{dx^2} = \frac{f_{i+1} - 2f_i + f_{i-1}}{h^2} \tag{III. 7}$$

We call eq. (III.6) and eq. (III.7) *central difference scheme* of the first and the second derivatives of the function f, respectively.

II.2 Common numerical schemes

Forward difference scheme:

This scheme approximates the derivative at a point by using the function values at that point and a nearby point ahead of it. It can be expressed as:

$$\frac{df(x)}{dx} = \frac{f(x+h) - f(x)}{h} \tag{III. 8}$$

Forward differences are useful in solving ordinary differential equations through single-step predictor-corrector methods such as Euler and Runge-Kutta methods [2].

Backward difference scheme:

Similar to the forward difference scheme, but it uses a nearby point behind the point of interest. It can be expressed as

$$\frac{df(x)}{dx} = \frac{f(x) - f(x-h)}{h} \tag{III. 9}$$

Backward differences become valuable when approximating derivatives in cases where future data remains unavailable.

First and second order central difference schemes:

This is the quotient we have seen before; it is commonly favored for its accuracy in comparison to backward and forward schemes. This scheme uses points both ahead and behind the point of interest to approximate the first and the second derivative.

Central differences are useful in solving partial differential equations.

Five-Point Stencil:

It is a more accurate scheme, often used in two-dimensional problems [3]. It consists on using four adjacent points in addition to the point of interest. Theses approximations are expressed as:

$$\frac{df}{dx} = \frac{-f(x+2h) + 8f(x+h) - 8f(x-h) + f(x-2h)}{12h} \tag{III. 10}$$

$$\frac{d^2f}{dx^2} = \frac{-f(x+2h) + 16f(x+h) - 30f(x) + 16f(x-h) - f(x-2h)}{12h^2} \tag{III. 11}$$

III. The hydrogen Atom Model

The significance of studying the hydrogen atom extends far beyond its historical roots. Though its spectra had a big impact in the early quantum theory, research involving the hydrogen remains at the cutting edge of science and technology. Investigations into hydrogen transitions have provided insights into fundamental constants across cosmic timescales. Additionally, it stands out as one of the rare realistic systems that can be solved analytically [4].

In this chapter we will use the hydrogen as a model to solve the time independent MSE for a single electron interacting with a nucleus containing only one proton, which acts as a central potential.

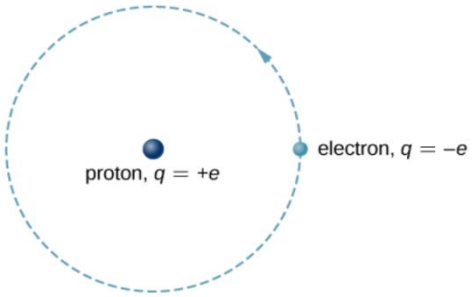

Figure III.2: The hydrogen model

Potential energy of the electron-proton system in hydrogen atom is basically the coulombic potential:

$$V(r) = -\frac{e^2}{4\pi\varepsilon_0 r} \qquad \text{(III. 12)}$$

The time independent MSE, which we have obtained in the second chapter, was written as:

$$\hat{H}\psi = E\psi \qquad \text{(III. 13)}$$

The wave function of the hydrogen atom, in spherical coordinates (r, θ, ϕ), is expressed as:

$$\psi(\vec{r}) = \psi(r, \theta, \phi) \qquad \text{(III. 14)}$$

By separating the radial part $R(r)$from the angular part (due to the spherical symmetry of the problem), we can simplify the equation and focus only on solving for the radial component independently:

$$\psi(\vec{r}) = R(r)Y_l^{m_l}(\theta,\phi) \qquad \text{(III. 15)}$$

where $Y_l^{m_l}(\theta,\phi)$represents the spherical harmonics and $-l \le m_l \le +l$

The well known radial Schrodinger equation is expressed in the following form [4]:

$$\frac{d}{dr}\left(r^2\frac{dR(r)}{dr}\right)+\frac{2mr}{\hbar^2}\left(\frac{e^2}{4\pi\varepsilon_0}\frac{1}{r}-\frac{l(l+1)}{2mr^2}\hbar^2+E\right)R(r)=0 \qquad \text{(III. 16)}$$

The radial part $R(r)$ depends on *l*and *n*, the orbital angular momentum quantum number and the principal quantum number, respectively.

IV. Resolution of the Radial Schrodinger Equation

In this section, we will proceed to solve the radial Schrodinger equation numerically with finite difference scheme.

$$\frac{d}{dr}\left(r^2\frac{dR(r)}{dr}\right)+\frac{2mr}{\hbar^2}\left(\frac{e^2}{4\pi\varepsilon_0}\frac{1}{r}-\frac{l(l+1)}{2mr^2}\hbar^2+E\right)R=0 \qquad \text{(III. 17)}$$

We set$\boldsymbol{\rho = rR(r)} \implies \boldsymbol{R(r)} = {}^{\boldsymbol{\rho}}/_{\boldsymbol{r}}$ and making a substitution in eq. (III.17), we consider only the first term:

$$\frac{d}{dr}\left(r^2\frac{dR}{dr}\right)=\frac{d}{dr}\left(r^2\frac{d\left({}^{\rho}/_{r}\right)}{dr}\right)=\frac{d}{dr}\left(r\frac{d\rho}{dr}-\rho\right)=r\frac{d^2\rho}{dr^2}$$

$$\frac{d}{dr}\left(r^2\frac{dR}{dr}\right)=r\frac{d^2\rho}{dr^2} \qquad \text{(III. 18)}$$

Substituting eq. (III.18) in eq. (III.17), we obtain:

$$r\frac{d^2\rho}{dr^2}+\frac{2mr}{\hbar^2}\left(\frac{e^2}{4\pi\varepsilon_0}\frac{1}{r}-\frac{l(l+1)}{2mr^2}\hbar^2+E\right)\rho=0 \qquad \text{(III. 19)}$$

Dividing eq. (III.19) by the variable *r*, we obtained the final form of radial SE (independent on time) as:

$$\frac{d^2\rho}{dr^2}+\frac{2m}{\hbar^2}\left(\frac{e^2}{4\pi\varepsilon_0}\frac{1}{r}-\frac{l(l+1)}{2mr^2}\hbar^2+E\right)\rho=0 \qquad \text{(III. 20)}$$

IV.1 *Finite difference method (FDM)*

As shown previously, we subdivide the axis of the variable r into a grid of n points (Figure III.3). The position r becomes r_i:

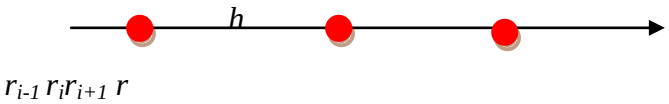

Figure III.3: One-dimensional grid, $\Delta r = r_{i+1} - r_i = h$represents the step of subdivision

We rewrite the eq. (III.20) in this way,

$$-\frac{\hbar^2}{2m}\frac{d^2\rho}{dr^2} - \frac{e^2}{4\pi\varepsilon_0}\frac{1}{r}\rho + \frac{l(l+1)}{2mr^2}\hbar^2\rho = E\rho$$

This previous equation can be written as:

$$H\rho = E\rho \qquad \text{(III. 21)}$$

Where H represents a matrix composed of*three matrix*, that we should compute:

$$H = -\frac{\hbar^2}{2m}(mat1 - mat3) - mat2 \qquad \text{(III. 22)}$$

Computation of the Laplacian term (matrix called mat1):

The first term in eq. (III.20) is noted:

$$term1 = \frac{\partial^2\rho}{\partial r^2}$$

The application of the approximating the second derivative using the central difference quotient leads to:

$$\frac{d^2\rho_i}{dr^2} = \frac{\rho_{i+1} - 2\rho_i + \rho_{i-1}}{\Delta r^2}$$

We increment the index $i = 1, n \quad \Rightarrow$

$$\begin{cases} i = 1 & \frac{d^2\rho_1}{dr^2} = \frac{1}{h^2}(\rho_2 - 2\rho_1 + \rho_0) \\ i = 2 & \frac{d^2\rho_2}{\partial r^2} = \frac{1}{h^2}(\rho_3 - 2\rho_2 + \rho_1) \\ i = 3 & \frac{d^2\rho_3}{dr^2} = \frac{1}{h^2}(\rho_4 - 2\rho_3 + \rho_2) \\ i = 4 & \frac{d^2\rho_4}{dr^2} = \frac{1}{h^2}(\rho_5 - 2\rho_4 + \rho_3) \\ & \vdots \\ & \vdots \\ i = n & \frac{d^2\rho_n}{dr^2} = \frac{1}{h^2}(\rho_{n+1} - 2\rho_n + \rho_{n-1}) \end{cases}$$

The final result is a matrix written as follows:

$$mat1 = \begin{pmatrix} -2 & 1 & 0 & 0 & 0 \dots \\ 1 & -2 & 1 & 0 & 0 \dots \\ 0 & 1 & -2 & 1 & 0 \dots \\ \dots & \dots & \dots & \dots & \dots \\ 0 & 0 & 0 \dots & 1 & -2 \end{pmatrix} \qquad \text{(III. 23)}$$

The implementation of the first matrix in eq. (III.23) in Python code is given bellow:

```
defcalcul_laplacian(n):
    fori in range(n):
        for j in range(n):
            if (i==j):
                mat1[i][j] =-2/h**2
            elif (abs(i-j) ==1):
            mat1[i][j] =1/h**2
             else:
            mat1[i][j] =0
return mat1
```

Computation of the potential term (matrix called mat2):

$$term2 = \frac{e^2}{4\pi\varepsilon_0}\frac{1}{r}\rho \quad \longrightarrow term2 = \frac{e^2}{4\pi\varepsilon_0}\frac{1}{r_i}\rho_i$$

"mat2" has the form of the following matrix:

$$mat2 = \frac{e^2}{4\pi\varepsilon_0}\begin{pmatrix} 1/r_1 & 0 & 0 & 0 & 0 \dots \\ 0 & 1/r_2 & 0 & 0 & 0 \dots \\ 0 & 0 & 1/r_3 & 0 & 0 \dots \\ \dots & \dots & \dots & \dots & \dots \\ 0 & 0 & 0 \dots & 0 & 1/r_n \end{pmatrix} \qquad \text{(III. 24)}$$

The implementation of the second matrix in eq. (III.24) in Python:

```
defcalcul_potential(r):
    fori in range(n):
        for j in range(n):
            if (i==j):
                mat2[i][j] =e**2/(4*pi*epsilon_0*r[i])
            else:
                mat2[i][j] =0
return mat2
```

Computation of the angular term (mat3):

$$term3 = \frac{l(l+1)}{r^2} \quad \longrightarrow \quad term3 = l(l+1)\frac{1}{{r_i}^2}$$

$$mat3 = l(l+1)\begin{pmatrix} {}^{1}/_{{r_1}^2} & 0 & 0 & 0 & 0 \dots \\ 0 & {}^{1}/_{{r_2}^2} & 0 & 0 & 0 \dots \\ 0 & 0 & {}^{1}/_{{r_3}^2} & 0 & 0 \dots \\ \dots & \dots & \dots & \dots & \dots \\ 0 & 0 & 0 \dots & 0 & {}^{1}/_{{r_n}^2} \end{pmatrix} \qquad \text{(III. 25)}$$

The implementation of the third matrix in eq. (III.25) in Python:

```
defcalcul_angular(r):
fori in range(n):
    for j in range(n):
        if (i==j):
            mat3[i][j] =(l*(l+1.))/(r[i]**2)
else:
            mat3[i][j] =0
 return mat3
```

Computation of the Hamiltonian term (H matrix):

$$H = -\frac{\hbar^2}{2m}\left(\begin{pmatrix} -2 & 1 & 0 & 0 & 0\dots \\ 1 & -2 & 1 & 0 & 0\dots \\ 0 & 1 & -2 & 1 & 0\dots \\ \dots & \dots & \dots & \dots & \dots \\ 0 & 0 & 0\dots & 1 & -2 \end{pmatrix} - l(l+1)\begin{pmatrix} 1/r_1{}^2 & 0 & 0 & 0 & 0\dots \\ 0 & 1/r_2{}^2 & 0 & 0 & 0\dots \\ 0 & 0 & 1/r_3{}^2 & 0 & 0\dots \\ \dots & \dots & \dots & \dots & \dots \\ 0 & 0 & 0\dots & 0 & 1/r_n{}^2 \end{pmatrix}\right)$$

$$-\frac{e^2}{4\pi\varepsilon_0}\begin{pmatrix} 1/r_1 & 0 & 0 & 0 & 0\dots \\ 0 & 1/r_2 & 0 & 0 & 0\dots \\ 0 & 0 & 1/r_3 & 0 & 0\dots \\ \dots & \dots & \dots & \dots & \dots \\ 0 & 0 & 0\dots & 0 & 1/r_n \end{pmatrix} \quad \text{(III. 26)}$$

The implementation of the H matrix (Hamiltonian eq. (III.26)) in Python:

```
defHamiltonian(r):
    mat1 = calcul_laplacian(n)
    mat2 = calcul_potentiel(r)
    mat3 = calcul_angular(r)
    H = -hbar**2 / (2.0 * m_e) * (mat1 - mat3) -mat2  #
return H
```

The final step is the diagonalization of the matrix H to solve the eigen problem. Its eigenvalues directly correspond to the energy states *E*, while the associated eigenvectors ρ are linked to the radial part of the hydrogen wave function *R* through the simple substitution we adopted previously: $\rho = rR$.

We have used the following Python script to solve the eigen problem:

```
#solving the eigenproblem
number_eigenvalues=10
eigenvalues, eigenvectors = eigs(H, k=number_eigenvalues, which='SM')
eigenvectors = np. array ([x for _, x in sorted (zip (eigenvalues, eigenvectors. T),
key=lambda pair: pair [0])])
eigenvalues = np. sort(eigenvalues)
```

We used the following Python script to calculate wave function and plot the densities of probabilities:

```
densities = [np. absolute (eigenvectors [i, :]) **2 for i in range(len(eigenvalues))]
#PLOT
energies = ['E = {: >5.2f} eV'. format(eigenvalues[i]. real / e) for i in range (3)]
plt.plot(r * 1e+10, densities [0], color='green', label=energies [0])
plt.plot(r * 1e+10, densities [1], color='red', label=energies [1])
plt.plot(r * 1e+10, densities [2], color='blue',label=energies [2])
plt.xlabel('r')
plt.ylabel('probability density')
plt.legend()
plt.show()
```

Remarks: some modules are required for Python3.4 (and more), numpy, scipy and matplotlib modules.

V. Results and discussions

In this section, we give first, the radial wave function computed numerically by the performed code written in Python and we add the temporal compound of MSE. In order to make a comparison, results obtained by classical SE are also presented.

The fundamentals constants used in our program are:

$$\begin{cases} \hbar = 1.054571817 \times 10^{-34}\ \text{J.s} \\ m_e = 9.1093837 \times 10^{-31}\ \text{kg} \\ \varepsilon_0 = 8.854188 \times 10^{-12}\text{Fm}^{-1} \\ e = 1.60217662 \times 10^{-19}\text{C} \end{cases}$$

The relaxation time is of value $\tau = 1.208 \times 10^{-17}\text{s}$

For the angular momentum quantum number *l*=0, we exanimate the hydrogen s states (1s, 2s, 3s, ...). The corresponding energies obtained align with the expected values of the first 3 states which are:

$$\mathrm{E}_1 = -\frac{13.6\text{eV}}{1^2} = -13.6\ \text{eV}$$
$$\mathrm{E}_2 = -\frac{13.6\text{eV}}{2^2} = -3.4\ \text{eV}$$
$$\mathrm{E}_3 = -\frac{13.6\text{eV}}{3^2} = -1.51\ \text{eV}$$

The following graph (figure III.4) represents the function $\rho(r)$ which we previously set as $\rho(r) = rR(r)$.

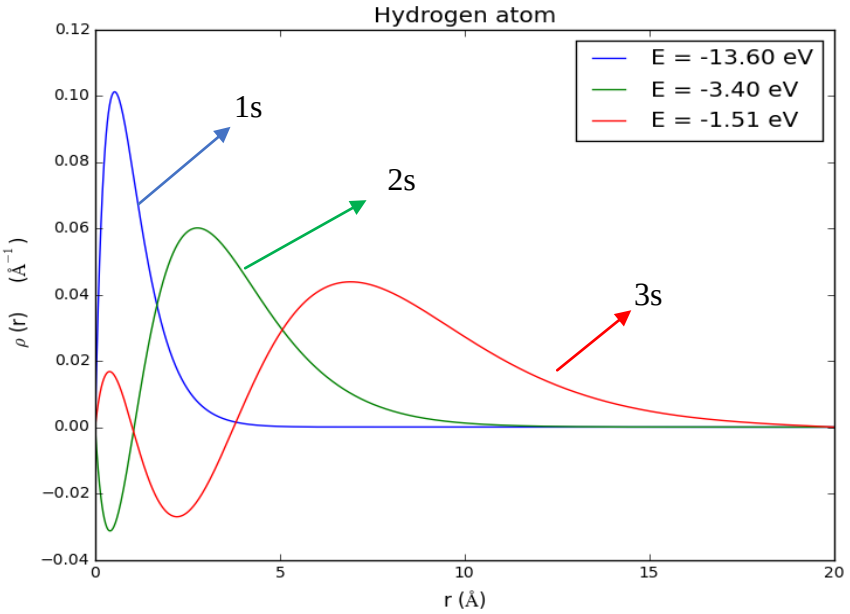

Figure III.4: $\rho(r)$ for *l*=0, and for 3 different states

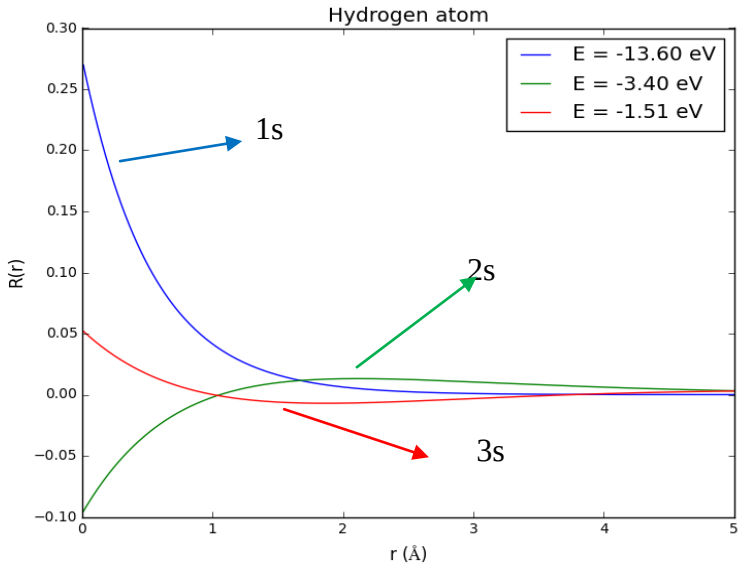

Figure III.5: variation of radial part R(r) of wave function of the hydrogen atom for *l*=0and for 3 different states

In following and for analysis, we combined the analytical temporal solution obtained in the second chapter with the numerical radial solutions obtained from our numerical computations. By doing so, we were able to plot the results to visualize the electron behavior over time.

Specifically, we compared the standard Schrödinger equation with the MSE, allowing us to observe the differences in the system's dynamics.

The graphs in Figure III.6 illustrate these comparisons, highlighting the effects of the ultrashort pulses on the system.

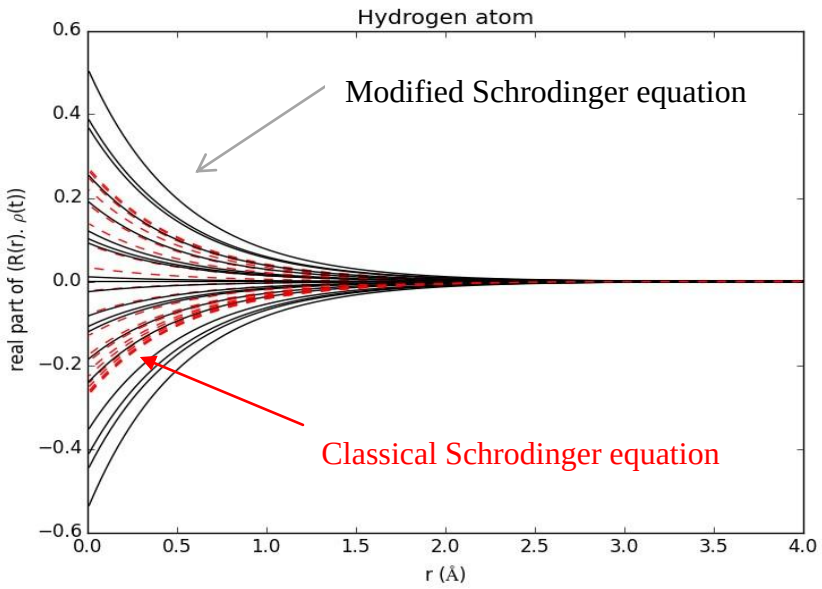

Figure III.6: The evolution of the real part of the $R(r)\varphi(t)$for several times, for*l*=0, E=-13.60eV. The black curve represents the results of MSE and the red curve represents the results of the classical SE

The probability of finding particle in a volume $dv = r^2 \sin\theta dr d\theta d\phi$, is defined by the following relation:

$$P_{nl}(r)dr = \int_0^{2\pi} \int_0^{\pi} |\psi_{nlm}(\vec{r})|^2 r^2 \sin\theta dr d\theta d\phi \qquad \text{(III. 26)}$$

The probability of density is illustrated in the figure III.7 for several values of time.

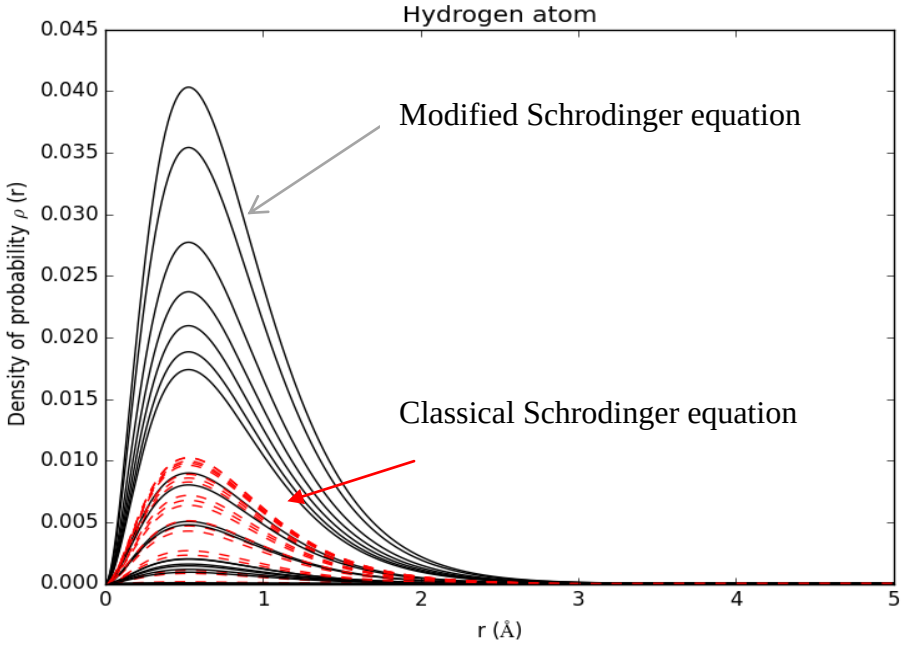

Figure III.7: Density of probability for several values of times and for *l*=0, E=-13.6 eV.
The black curve represents the results of MSE and the red curve represents the results of the classical SE.

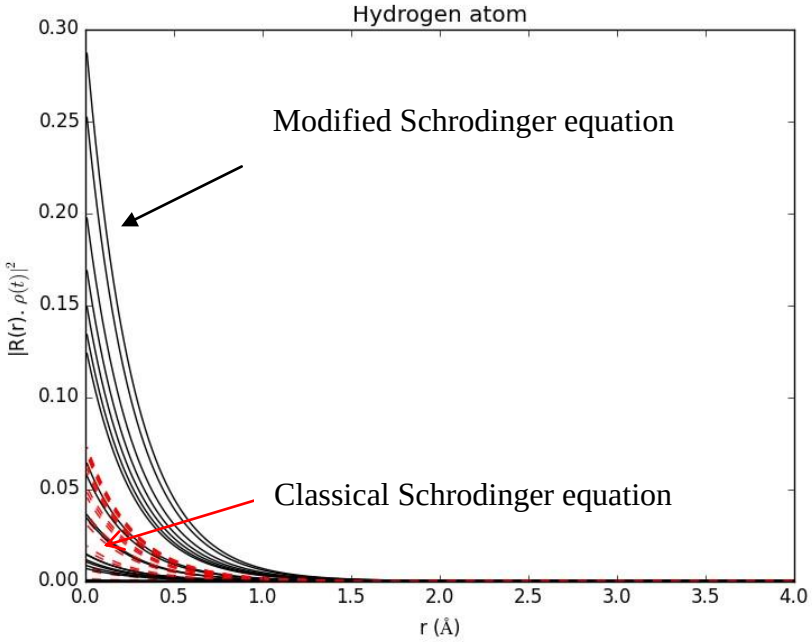

Figure III.8: $|R(r)\varphi(t)|^2$ for several values of times and for *l*=0, E=-13.6 eV.
The black curve represents the results of MSE and the red curve represents the results of the classical SE.

Interpretation:

The figure III.6, III.7 and III.8 displays a comparative analysis of the results from the classical Schrodinger equation and its modified version. The graph in figure III.8 shows that the probability density for the MSE exhibits significant enhancements compared to the classical equation. This indicates that the presence of attosecond pulses provides a clearer, more detailed visualization of electron positions and movements.

For $l = 1$, the first three states correspond to the first three possible values of n (the principal quantum number) which are 2p, 3p and 4p, the corresponding energies obtained in figure (III.7) also align with the expected values of the first 3 states which are:

$$E_2 = -\frac{13.6\ \text{eV}}{2^2} = -3.4\ \text{eV}$$

$$E_3 = -\frac{13.6\ \text{eV}}{3^2} = -1.51\ \text{eV}$$

$$E_4 = -\frac{13.6\ \text{eV}}{4^2} = -0.85\ \text{eV}$$

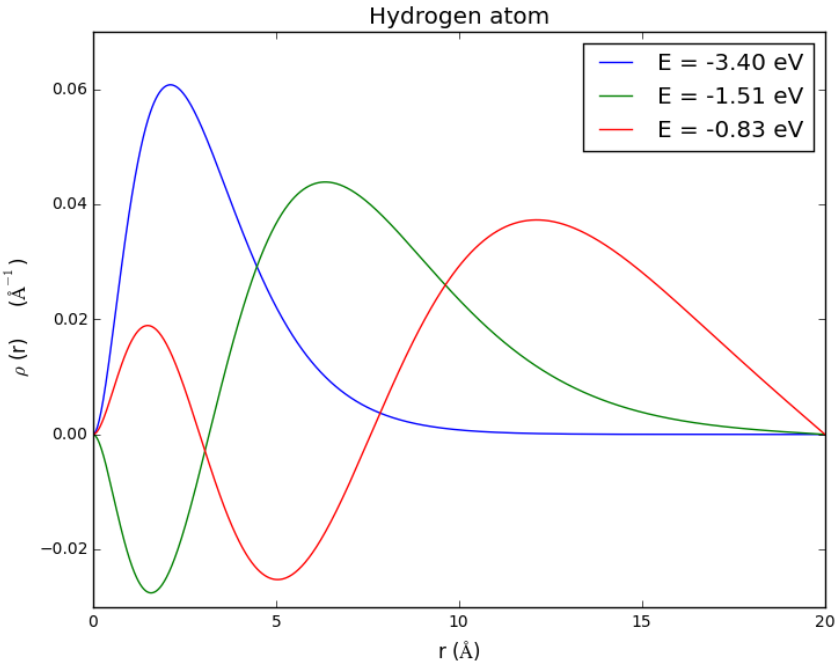

Figure III.9: $\rho(r)$ for $l = 1$, and for 3 different modes (states)

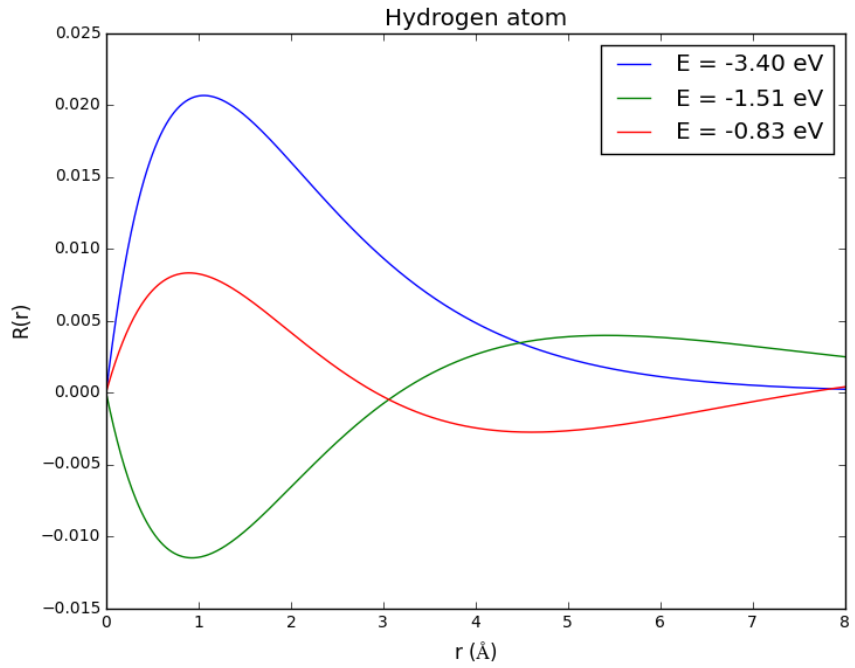

Figure III.10: Radial wave function R(r) of the hydrogen atom for $l = 1$ and for 3 different states

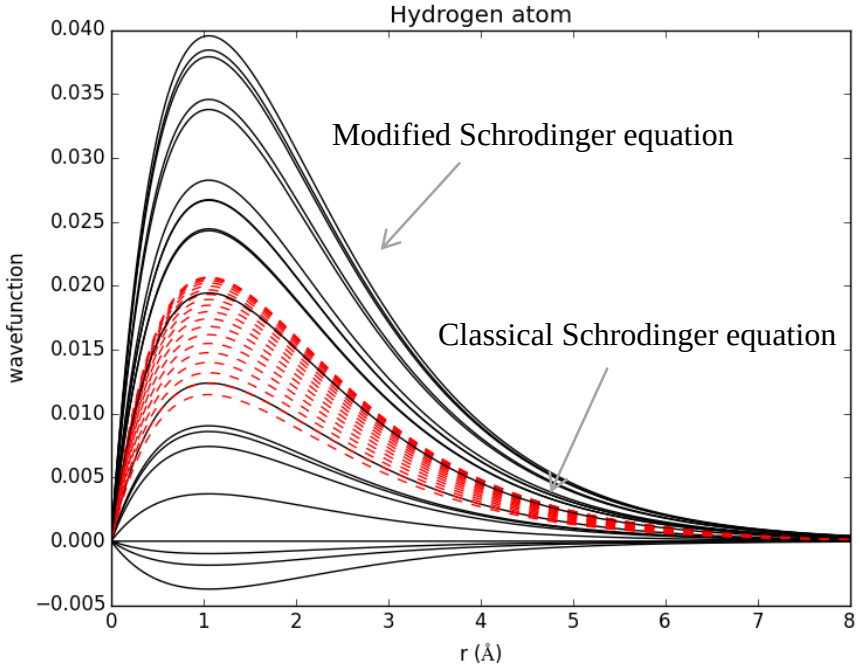

Figure III.11: The radial wavefunction evolution for several times for $l = 1, E = -3.40$ eV. The black curve represents the results of MSE and the red curve represents the results of the classical SE

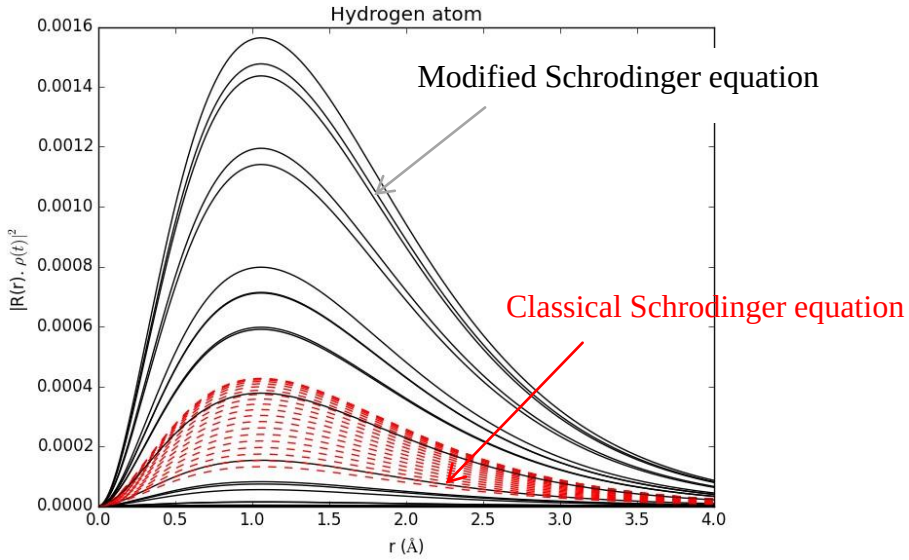

Figure III.12: $|R(r)\varphi(t)|^2$ for several timesand for $l = 1, E = -3.40$ eV.
The black curve represents the results of MSE and the red curve represents the results of the classical SE

Interpretation:

The Figures III.11 and III.12 presents a comparative analysis of the classical Schrödinger equation and its modified version for a higher energy state, providing a clearer observation of the distinction between the two results. That validates the fact that under the influence of attosecond pulses, the probability density exhibits a significant improvement.

To complement our study, the following figures present three-dimensional representations of the wave functions and probability densities derived from both the standard and modified Schrödinger equations. These visualizations offer a more comprehensive view of the spatial characteristics and differences between the two models.

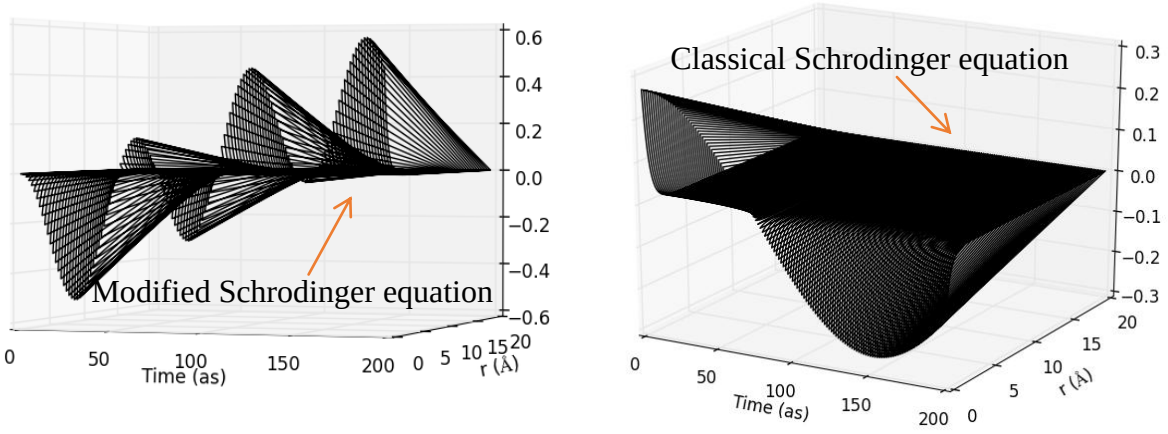

Figure III.13: Three-Dimensional visualizations of classical Schrodinger and modified Schrodinger equations for $E = -13.60$ eV: wave functions

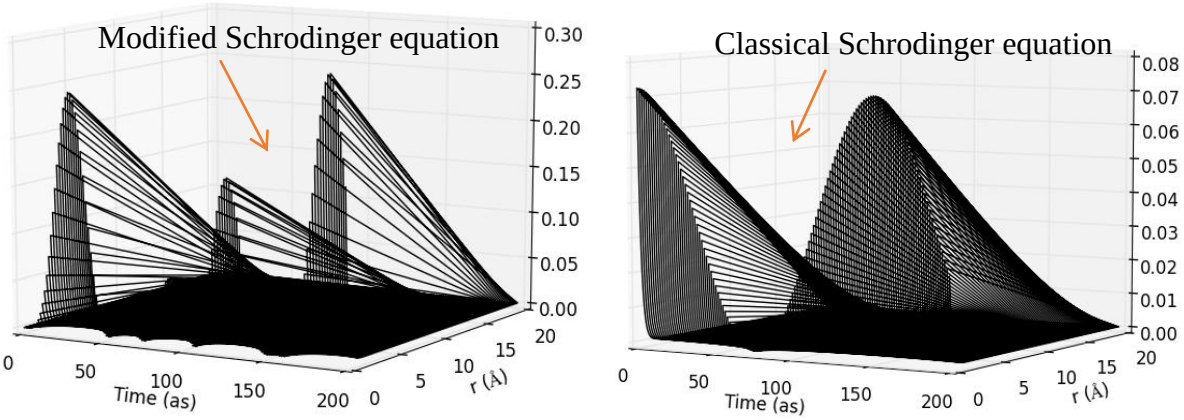

Figure III.14: Three-Dimensional visualizations of classical Schrodinger and modified Schrodinger equations for $E = -13.60$ eV: Probability densities

VI. Conclusion

In this chapter, we successfully solved the Radial Schrödinger equation numerically using the finite difference method. Building on this, we integrated the Temporal Solution, derived analytically in the previous chapter, with our numerical results.

Our results, plotted for various wave functions and probability densities corresponding to different angular momentum quantum numbers *l*, consistently demonstrate the significant impact of attosecond pulses. The probability densities are notably enhanced under the modified Schrödinger equation, validating its effectiveness in capturing electron behavior on the attosecond timescale.

REFERENCES of Chapter III

[1] Chapter6: The finite difference method,laboratory of Jacques-Louis Lions. source:https://www.ljll.fr/~frey/cours/UdC/ma691/ma691_ch6.pdf
[2] Timothy Sauer of George Mason University, numerical analysis, second editionpearson. p. 244 and p 259, 978-0-321-78367, (2011).
[3] Schwarzschild, "Optical Frequency Measurement is Getting a Lot More Precise," Physics Today 50(10) 19–21 (1997).
[4] Physical chemistry for the biosciences, Raymond Chang,LibreTextsTextmap, p. 426-432 (2024).

General Conclusion :

In this study, we have explored the interaction between attosecond laser pulses and matter, employing both theoretical approaches and numerical simulations to understand and visualize electron dynamics at an unprecedented temporal resolution.

We started by presenting the generation of attosecond pulses through the process of high harmonic generation (HHG). Using the semi-classical model, we analyzed this phenomenon, providing insights into both the classical and quantum descriptions of HHG. We also highlighted various applications of attosecond pulses, demonstrating its significance in advancing our understanding of ultrafast phenomena.

In the second chapter, we focused on the theoretical frameworks that describe the interaction of attosecond lasers with matter. We started with the quantum heat equation, an essential tool for describing the heat transfer in the context of ultrashort pulses, where traditional Fourier laws fail. Additionally, we derived the modified Schrödinger equation from the quantum heat equation and solved it using the method of separation of variables. This allowed us to handle both temporal and spatial components, solving the temporal part analytically.

We further explored the modified Klein-Gordon equation, offering another model for describing the temperature of electron under the influence of attosecond pulses.

In third chapter, we addressed the numerical solutions of the modified Schrödinger equation (MSE). Using the finite difference method in python, we solved the radial position component and integrated our analytical temporal solution. Our results, plotted for various wave functions and probability densities corresponding to different angular momentum quantum numbers l, consistently demonstrate the significant impact of attosecond pulses. We have observed a notable increase in density within the modified Schrödinger equation compared to the classical one. This heightened density validated the efficacy of attosecond pulses in providing clearer visualizations of electron motion, aligning with the fundamental principle that these ultrafast pulses are well-suited to capture elementary electron dynamics.

Annex 1

The python script for generating a femtosecond pulse train (intensity)

```
#####
import numpy as np
import matplotlib.pyplot as plt
fr=20.e12
omega=2*np.pi*fr   #frequence de répétition
N=20     #number of iterations
Fichier=open("Femto.dat","w")
y = lambda x: (np.sin((N-1)*omega*x/2))**2/(np.sin(omega*x/2))**2
t = np.arange(-120, 120, 0.01)  #  commande de partage (debut, fin, pas)
t=t*1.e-15
for i in range (0,len(t)):
Fichier.write("%f      %s     \n" % (t[i]*1e15, y(t[i])))
Fichier.close()
plt.plot(  t*1.e15,y(t),'k',linewidth= 2)
plt.title('signal impusionnel ')
plt.xlabel('t  fs')
plt.ylabel('  Intensité (u.a) ')
plt.show()
```

Annex 2

The python script Plotting potential Tunnel Effect

```
import matplotlib.pyplot as plt
import numpy as np
def V(x,E):
    V=-Zeff/x+x*E
    return V
def V1(x,E):
    V1=Zeff/x+x*E
    return V1
x1=np.linspace(-15,-0.1,60)
x2=np.linspace(0.1,15,60)
x=[ ]
for i in range(len(x1)):
    x.append(x1[i])
for i in range(len(x2)):
    x.append(x2[i])
Zeff=1
E=0., E1=0.1, E2=-0.1
y=[ ]
#second tableaux E positif
w=[ ]
#second tableaux E négatif
u=[ ]
for i in range(len(x1)):
    z=V1(x1[i],E)
    y.append(z)
for i in range(len(x2)):
    z=V(x2[i],E)
    y.append(z)
#
for i in range(len(x1)):
    z=V1(x1[i],E1)
    w.append(z)
for i in range(len(x2)):
    z=V(x2[i],E1)
    w.append(z)
#
for i in range(len(x1)):
    z=V1(x1[i],E2)
    u.append(z)
for i in range(len(x2)):
    z=V(x2[i],E2)
    u.append(z)
filename = "graphe"
#
fig, ax = plt.subplots()
ax.plot(x,y, 'k',linewidth=3)
ax.plot(x,w,'r--',linewidth=3)
ax.plot(x,u, 'b:',linewidth=2)
plt.legend(['E=0' ,'E= 0.1','E= - 0.1'],loc='lower right', fontsize=11,frameon=True)
plt.ylim(-4,1.5)
plt.xlim(-11,11)
plt.xlabel("x (u.a)")
plt.ylabel(" Potentiel  V(x)   (u.a)")
plt.tick_params(labelsize=12)
plt.savefig(filename+'.png')
plt.show()
```

ANNEX 3

Derivation of the Standart Schrodinger equation (SE)

Starting with the Helmholtz equation

$$\left(\Delta + \frac{n\omega^2}{c^2}\right)\psi(\vec{r}) = 0 \qquad we\ set\ that\ \ k^2 = \frac{n\omega^2}{c^2}$$

We set $\lambda = {}^{2\pi}/_{k}$ then :

$$\left(\Delta + \frac{4\pi^2}{\lambda^2}\right)\psi(\vec{r}) = 0 \qquad (A.1)$$

According to the de Broglie relation, the impulse is written as: $p = mv \quad , \quad \lambda = {}^{h}/_{p}$

$$\Longrightarrow \quad \lambda = \frac{h}{mv} \quad \Longrightarrow \quad \frac{1}{\lambda^2} = \frac{m^2v^2}{h^2} \qquad (A.2)$$

Substituting (2) in (1):

$$\left(\Delta + 4\pi^2\frac{m^2v^2}{h^2}\right)\psi(\vec{r}) = 0 \qquad (A.3)$$

The total energy E can be expressed as:

$$E = \frac{1}{2}mv^2 + V(r) \quad \Longrightarrow \quad mv^2 = 2\big(E - V(r)\big) \quad (A.4)$$

Substituting (4) in (3) :

$$\left(\Delta + \frac{8\pi^2 m}{h^2}(E - V(r))\right)\psi(\vec{r}) = 0$$

$$\hbar = \frac{h}{2\pi} \quad \Longrightarrow \left[\Delta + \frac{2m}{\hbar^2}\big(E - V(r)\big)\right]\psi(\vec{r}) = 0 \qquad (A.5)$$

Eq. (A.5) represents the time independent Schrodinger equation.

The general solution of the time dependent Schrodinger equation has the following form:

$$\Psi(\vec{r}, t) = \psi(\vec{r})\ e^{-i\frac{E}{\hbar}t} \qquad (A.6)$$

$$\frac{\partial\Psi(\vec{r}, t)}{\partial t} = -i\frac{E}{\hbar}\psi(\vec{r})e^{-i\frac{E}{\hbar}t} \quad \Longrightarrow \ E\psi(\vec{r}) = i\hbar\frac{\partial\Psi(\vec{r}, t)}{\partial t}e^{i\frac{E}{\hbar}t} \quad (A.7)$$

Replacing (A.6) and (A.7) in (A.5), we obtain the time dependent Schrödinger equation:

$$\boldsymbol{i\hbar\frac{\partial\Psi(\vec{r}, t)}{\partial t} = -\frac{\hbar^2}{2m}\frac{\partial^2\Psi(\vec{r}, t)}{\partial r^2} + V(r)\Psi(\vec{r}, t)} \qquad (A.8)$$

Abstract: We have studied the interaction of attosecond laser pulses with matter and the significance of these ultrashort pulses in capturing electron dynamics. We introduced the generation of attosecond pulses through the process known as high harmonic generation (HHG), described using the three-step semi-classical model. We discussed theoretical models that serves as the main pillars of understanding the interaction of ultrashort pulses with mattersuch as the quantum heat transfer equation (QHT) and the modified Schrödinger equation (MSE), to describe the interaction of attosecond lasers with matter. Analytical and numerical solutions of the modified Schrödinger equation demonstrate the impact of attosecond pulses on electron motion, validating the efficacy of these pulses in providing clearer visualizations of electron dynamics. Overall, our study shows the significance of attosecond pulses in advancing our understanding of ultrafast processes, aligning with the fundamental principle that these ultrafast pulses are well-suited to capture elementary electron dynamics.

Key words:Interaction of attosecond pulses with matter, high harmonic generation, Quantum heat equation, modified Schrodinger equation, Hydrogen atom.

ملخّص:لقد درسنا تأثير نبضات الليزر الأتوثانيةعلى المادّة وأهمية هذه النبضات فائقة القصر في تصوير ديناميكيات الإلكترونات. قدّمنا كيف يتمّ توليد نبضات الأتوثانية من خلال عملية تعرف بتوليد التوافقيات العالية، التي تم وصفها باستخدام النموذج شبه الكلاسيكي الثلاثي الخطوات. ناقشنا النماذج النظرية التّي تعتبر الركائز الأساسية لفهم تأثير النبضات فائقة القصر على المادّة، مثل معادلة الانتقال الحراري الكميةومعادلةشرودينغرالمعدّلة. أظهرت الحلول التحليلية والعددية التي تمّت حسابتها عن طريق البرمجة الرقمية لمعادلة شرودنغر المعدلة تأثير النبضات الأتوثانية على حركة الإلكترونات، مما يؤكد فعالية هذه النبضات في توفير تصورات أوضح لديناميكيات الإلكترونات. بشكل عام، تُظهر دراستنا أهمية النبضات الأتوثانية في تقدم فهمنا للظواهر فائقة السرعة، بما يتماشى مع المبدأ الأساسي بأن هذه النبضات فائقة السرعة مناسبة تمامًا لالتقاط الديناميكيات الأساسية للإلكترونات.

الكلمات المفتاحية: تأثير نبضات الأتوثانية مع المادّة، توليد التوافقيات العالية، معادلة الانتقال الحراري الكمية، معادلة شرودنغر المعدلة، ذرّة الهيدروجين.

Resumé: Nous avons étudié l'interaction des impulsions laser attosecondes avec la matière et l'importance de ces impulsions ultra-courtes dans la capture de la dynamique des électrons. Nous avons introduit la génération d'impulsions attosecondes par le processus connu sous le nom de génération d'harmoniques élevés (GHE), décrit à l'aide du modèle semi-classique en trois étapes. Nous avons discuté des modèles théoriques qui servent de principaux piliers pour comprendre l'interaction des impulsions ultra-courtes avec la matière, tels que l'équation de transfert de chaleur quantique (QHT) et l'équation de Schrödinger modifiée (MSE), pour décrire l'interaction des lasers attosecondes avec la matière. Les solutions analytiques et numériques de l'équation de Schrödinger modifiée démontrent l'impact des impulsions attosecondes sur le mouvement des électrons, validant l'efficacité de ces impulsions pour fournir des visualisations plus claires de la dynamique des électrons. Dans l'ensemble, notre étude montre l'importance des impulsions attosecondes pour faire progresser notre compréhension des processus ultrarapides, en accord avec le principe fondamental selon lequel ces impulsions ultrarapides sont bien adaptées pour capturer la dynamique élémentaire des électrons.

Mots-clés : Interaction des impulsions attosecondes avec la matière, génération d'harmoniques élevés, équation de transfert de chaleur quantique, équation de Schrödinger modifiée, atome d'hydrogène.